Journal of Computational Physics **157,** 500–538 (2000)
doi:10.1006/jcph.1999.6383, available online at http://www.idealibrary.com on IDEAL®

Discretely Nonreflecting Boundary Conditions for Linear Hyperbolic Systems[1]

Clarence W. Rowley and Tim Colonius

Mechanical Engineering 104-44, California Institute of Technology, Pasadena, California 91125
E-mail: clancy@caltech.edu, colonius@caltech.edu

Received April 15, 1999; revised September 23, 1999

Many compressible flow and aeroacoustic computations rely on accurate nonreflecting or radiation boundary conditions. When the equations and boundary conditions are discretized using a finite-difference scheme, the dispersive nature of the discretized equations can lead to spurious numerical reflections not seen in the continuous boundary value problem. Here we construct discretely nonreflecting boundary conditions, which account for the particular finite-difference scheme used, and are designed to minimize these spurious numerical reflections. Stable boundary conditions that are local and nonreflecting to arbitrarily high order of accuracy are obtained, and test cases are presented for the linearized Euler equations. For the cases presented, reflections for a pressure pulse leaving the boundary are reduced by up to two orders of magnitude over typical ad hoc closures, and for a vorticity pulse, reflections are reduced by up to four orders of magnitude.

Key Words: nonreflecting boundary conditions; artificial boundary conditions; finite difference; Euler equations; high-order-accurate methods.

CONTENTS

[1] Supported in part by NSF Grant CTS-9501349. The first author gratefully acknowledges support under an NSF Graduate Fellowship. Part of this work was presented in preliminary form in AIAA Paper 98-2220.

0021-9991/00 $35.00

1. INTRODUCTION

It is well known that finite-difference models of nondispersive (hyperbolic) partial differential equations are themselves dispersive (see, e.g., [3, 26, 29]). This dispersive nature of finite-difference schemes has profound implications for the construction of accurate and stable artificial boundary conditions, as it can lead to spurious numerical reflections, which can be a large source of error for sensitive computations. For example, repeated spurious numerical reflections have been found to cause physically unrealistic self-forcing of the flow, in computations of convectively unstable mixing layers [4, 16]. Nevertheless, dispersion has been largely ignored in practical implementation of artificial boundary conditions for the Euler equations of gas dynamics [5, 7, 25]. While boundary conditions that account for the dispersive effects of discretization have been developed in some special cases [3, 24], there is no general formulation for linear hyperbolic systems such as the linearized Euler equations.

The goal of this paper is to present a generalized framework that we have developed for constructing *numerically* (or *discretely*) *nonreflecting boundary conditions*, which are designed to reduce reflections of spurious numerical waves. We present the method for a class of linear hyperbolic systems, with specific application to the linearized Euler equations of gas dynamics. The resulting boundary conditions are well posed, can be extended to arbitrarily high order-of-accuracy, and are naturally written as closures for derivatives normal to the boundary, so for implicit finite-difference schemes no other closure is necessary. Both physical reflections, due to local approximations in the dispersion relation, and spurious numerical reflections, due to dispersive effects at finite resolution, are addressed in this approach. There are some tradeoffs that depend on the specific problem under consideration—for the linearized Euler equations, for instance, using high-order numerical closures at the right boundary can increase the error from approximations in the dispersion relation—but in general we show that the performance of the boundary conditions is excellent.

This paper is organized as follows. In Section 2, we describe our procedure for constructing continuous (i.e., non-discretized) nonreflecting boundary conditions for linear hyperbolic systems. This analysis builds on the work of Engquist and Majda [5, 6], and more recent work by Giles [7] and Goodrich and Hagstrom [8, 9, 12]. We present the important parts of the analysis in a framework that is readily extended to the discrete case. We also discuss local approximations to the exact (nonlocal) boundary conditions, and demonstrate how a powerful theorem of Trefethen and Halpern [27] may be used to determine well-posedness of the approximate boundary conditions.

These continuous boundary conditions give very accurate results when discretized in a typical ad hoc way—i.e., when biased or one-sided finite-difference approximations are used where necessary for derivatives at or near the boundary. However, more robust and accurate discrete boundary conditions are derived in Section 3, by explicitly considering the dispersive nature of the finite-difference discretization at the outset. We first show how to distinguish physical solutions, which resemble solutions of the non-discretized equations, from spurious solutions, which behave qualitatively differently, and are merely artifacts of the numerical scheme used. This analysis builds on earlier work by Vichnevetsky [29]. We then construct boundary conditions that are *discretely* nonreflecting, in the sense that they prevent not only reflection of physical waves, but also reflection of spurious waves from a boundary. This approach was used by Colonius [3] to derive numerically nonreflecting

boundary conditions for one-dimensional systems, and here we show how to extend the analysis to the multidimensional case. The approach is, of necessity, restricted to particular finite-difference schemes, and we choose the Padé three-point central difference to illustrate the analysis. We conclude by showing the results of several test cases that illustrate the benefits and limitations of these schemes.

2. CONTINUOUS NONREFLECTING BOUNDARY CONDITIONS

Several distinct approaches have been used in deriving boundary conditions for linear hyperbolic systems. We briefly review the basic ideas—recent reviews [20, 22, 28] give further references to the relevant literature.

The first method involves so-called radiation boundary conditions [1], which are based on asymptotic expansions of the solution produced by a finite source region. Very accurate local and nonlocal boundary conditions based on this expansion have been developed for the wave equation (e.g., [10]), but radiation techniques for the linearized Euler equations [22, 23] are more limited. In a comparison [15] of many different boundary conditions, the accuracy of these conditions was found to be roughly comparable to Giles' boundary conditions, discussed below.

A second technique uses a perfectly matched layer to absorb waves leaving the computational domain. Such a technique was proposed by Hu [17], who reports problems with numerical instability, and further analysis and tests [9, 13] demonstrate persistent problems with well-posedness.

The third technique goes back to the early work of Engquist and Majda [5, 6] and involves the decomposition of the solution into Fourier/Laplace modes. Exact boundary conditions are then constructed by eliminating those modes that have a group velocity directed into the computational domain. The exact conditions are nonlocal in space and time—that is, they are not expressed as differential equations, but as integrals over all of space and time—but local approximations to these can be constructed. These involve rational function approximations to $\sqrt{1-z^2}$, where z is the (spatial) wavenumber in the direction tangent to the boundary divided by the frequency of the wave. Note that multiplication of a variable by $\sqrt{1-z^2}$ in Fourier space corresponds to a nonlocal operation in real space. The term $\sqrt{1-z^2}$ arises when the dispersion relation for acoustic waves is split into incoming and outgoing modes at a boundary. For the simple wave equation, Trefethen and Halpern have shown in [27] that a certain class of rational function approximations leads to stable boundary conditions. This class does *not* include Taylor series expansions about $z = 0$ higher than second-order. However, stable Padé approximations can be constructed which *reproduce* the Taylor series to arbitrarily high order. The Padé approximations are exact for normal waves and give the highest error for waves whose group velocity is tangent to the boundary.

Unfortunately, the extension of the results for the simple wave equation to the linearized Euler equations has not been straightforward. Giles [7] found that the second-order Taylor series expansions of the modified dispersion relation led to ill-posed boundary conditions. By an ad hoc procedure, Giles modified these conditions to obtain boundary conditions that are stable, but have limited accuracy.

More recently, Goodrich and Hagstrom [9] described inflow and outflow boundary conditions for the linearized Euler equations that are well posed for arbitrarily high accuracy. Hagstrom [12] has also developed a series of nonlocal boundary conditions and a local approximation that is equivalent to the Padé approximation to $\sqrt{1-z^2}$. Using a somewhat

different approach, described in more detail in Subsection 2.2.3, we have derived a similar hierarchy. Interestingly, the proof of well-posedness for our boundary conditions leads to conditions on rational function approximations to the square root that are identical to those derived for the simple wave equation by Trefethen and Halpern [27]. This opens the possibility of a wide variety of boundary conditions that may be specifically tailored to the problem at hand, e.g., to exactly eliminate reflections of waves at a specified angle to the boundary. We give an example of such a scheme in Section 4.

2.1. *General Theory*

Consider the system

$$u_t + Au_x + Bu_y = 0 \tag{2.1}$$

for $0 < x < L$, $y \in \mathbb{R}$, where A and B are $n \times n$ matrices and u is a vector with n components. We will assume that the system (2.1) is strongly hyperbolic, in the sense of [11], and we note that strictly hyperbolic and symmetric hyperbolic systems fall into this category. In this paper, we will further assume that A is invertible, as is the case for the Euler equations of gas dynamics when they are linearized about a nonzero uniform mean flow. This assumption does not hold for systems with characteristic boundary, such as Maxwell's equations, but we believe it will be possible to extend the techniques presented here to include many such systems (see Majda and Osher [21]).

In a traditional normal mode analysis, solutions of (2.1) are made up of n different modes, which propagate at different speeds. A crucial step in developing boundary conditions for (2.1) is determining the direction of propagation of each mode, and distinguishing which modes are "outgoing" and which are "incoming" at the boundary.

Splitting into rightgoing and leftgoing modes. If we take a Fourier transform in y, with dual variable ik, and a Laplace transform in t, with dual variable s, the system becomes

$$\hat{u}_x = -A^{-1}(sI + ikB)\hat{u}. \tag{2.2}$$

If we define $z = ik/s$, we may write

$$\hat{u}_x = -sM(z)\hat{u}, \tag{2.3}$$

where $M(z) = A^{-1}(I + zB)$. We wish to separate $\hat{u}$ into modes that are "rightgoing" and modes that are "leftgoing." Each of these modes corresponds to an eigenvalue of $M(z)$. A well known result in the theory of hyperbolic systems is that if l is the number of positive eigenvalues of A, then solutions of (2.1) are made up of l "rightgoing" modes and $(n - l)$ "leftgoing" modes. For wavelike solutions, "rightgoing" and "leftgoing" solutions correspond to waves with energy traveling in the $+x$ and $-x$ directions, respectively. Not all solutions to (2.1) are waves, so for non-propagating solutions, the terms "rightgoing" and "leftgoing" refer to the algebraic labeling from the theory of well-posedness (see [14]) where, for instance, "rightgoing" modes refer to all modes which must be specified at the left boundary in order to obtain a well-posed problem.

When $z = 0$, $M(z) = A^{-1}$, so eigenvalues of $M(0)$ are real and nonzero. Accordingly, the l rightgoing modes of (2.1) correspond to the eigenvalues of $M(z)$ that are positive for $z = 0$,

and the $(n-l)$ leftgoing modes correspond to the eigenvalues of $M(z)$ that are negative for $z=0$.

If the matrix $M(z)$ is diagonalizable,[2] then there exists a matrix $Q(z)$ which satisfies

$$QMQ^{-1} = \Lambda = \begin{pmatrix} \Lambda^{\mathrm{I}} & 0 \\ 0 & \Lambda^{\mathrm{II}} \end{pmatrix}, \tag{2.4}$$

where $\Lambda(z)$ is the matrix of eigenvalues of $M(z)$, arranged so that Λ^{I} is an $l \times l$ matrix that is positive-definite for $z=0$, corresponding to rightgoing solutions, and Λ^{II} is an $(n-l)\times(n-l)$ matrix that is negative-definite for $z=0$, corresponding to leftgoing solutions. (Henceforth, all matrices are functions of z unless otherwise noted, so we drop the explicit z dependence.)

Multiplying by Q, (2.3) becomes

$$Q\hat{u}_x = -s(QMQ^{-1})Q\hat{u}, \qquad \text{i.e., } f_x = -s\Lambda f, \tag{2.5}$$

where $f = Q\hat{u}$ are the characteristic coordinates. Now we may partition (2.5) into

$$\frac{\mathrm{d}}{\mathrm{d}x}\begin{pmatrix} f^{\mathrm{I}} \\ f^{\mathrm{II}} \end{pmatrix} = -s\begin{pmatrix} \Lambda^{\mathrm{I}} & 0 \\ 0 & \Lambda^{\mathrm{II}} \end{pmatrix}\begin{pmatrix} f^{\mathrm{I}} \\ f^{\mathrm{II}} \end{pmatrix},$$

where the f^{I} are now purely rightgoing modes and the f^{II} are leftgoing modes.

Exact nonreflecting boundary conditions. Once this distinction has been made, the correct nonreflecting boundary conditions follow immediately. Since there are no incoming modes at a nonreflecting boundary, at the left boundary $x=0$ there should be no rightgoing modes, so an exact nonreflecting boundary condition is

$$f^{\mathrm{I}} = 0, \qquad \text{at } x = 0.$$

At the right boundary, there should be no leftgoing modes, so an exact nonreflecting boundary condition is

$$f^{\mathrm{II}} = 0, \qquad \text{at } x = L.$$

To implement these boundary conditions, we must transform back to the original variables $\hat{u}$, and then take the inverse Fourier and Laplace transforms. It is convenient to partition Q in the same manner as f,

$$Q = \begin{pmatrix} Q^{\mathrm{I}} \\ Q^{\mathrm{II}} \end{pmatrix},$$

[2] All we really require is that the M be *block* diagonalizable in the form (2.4), such that rightgoing and leftgoing solutions are decoupled. Some theorems given in [11, 14] guarantee that for strongly hyperbolic systems, the matrix $M(ik/s)$ is always block diagonalizable for $\mathrm{Re}\, s > 0$, and always diagonalizable for wavelike solutions with $\mathrm{Re}\, s = 0$, except when waves are tangent to the boundary. For tangential waves, the matrix M is *not* block diagonalizable in the manner of (2.4), so in deriving the nonreflecting boundary conditions, we exclude this case. This exclusion does not create a problem, because energy from tangential waves stays at the boundary and does not propagate into the domain, so it is only necessary to check that the boundary conditions are well posed for tangential waves. The family of boundary conditions presented in Subsection 2.2 satisfies the uniform Kreiss condition (see, e.g., Higdon [14] and references therein) and is thus strongly well-posed.

where Q^{I} is a rectangular matrix of dimension $l \times n$, and Q^{II} has dimension $(n-l) \times n$, so that the boundary conditions become

$$\begin{aligned} Q^{\mathrm{I}}\hat{u} &= 0, \qquad \text{at } x = 0 \\ Q^{\mathrm{II}}\hat{u} &= 0, \qquad \text{at } x = L, \end{aligned}$$

which may be implemented by taking the inverse Fourier and Laplace transforms.

Implementation and approximation. Two difficulties arise in implementing the above boundary conditions. First, since the boundary condition is expressed in Fourier–Laplace (x, ik, s) space, and in many cases (e.g., the linearized Euler equations) the matrix of left eigenvectors $Q(z)$ contains non-rational functions of ik/s (e.g., square roots), when we transform back to physical (x, y, t) space, the boundary condition will be nonlocal in both space and time. From a computational perspective, we would prefer a local boundary condition, which may be obtained by approximating non-rational elements of $Q(z)$ by rational functions of z (e.g., Padé approximations).

A second difficulty is that when approximations are introduced, the resulting boundary conditions may be ill posed. The theory of well-posedness is discussed in detail in [11, 14, 18], and here we summarize some of the important points.

Well-posedness and reflection coefficients. Well-posedness may be viewed as a solvability condition: we must be able to solve for the incoming modes uniquely in terms of the outgoing modes. To investigate this approach, consider the equation

$$\hat{u}_x = -sM(z)\hat{u}$$

for $0 < x < L$, with boundary conditions

$$\begin{aligned} E^{\mathrm{I}}\hat{u} &= 0, \qquad \text{at } x = 0 \\ E^{\mathrm{II}}\hat{u} &= 0, \qquad \text{at } x = L, \end{aligned}$$

where E^{I} is an $l \times n$ matrix, E^{II} is an $(n-l) \times n$ matrix, $M(z)$ is given by (2.3), and l is the number of rightgoing modes (i.e., positive eigenvalues of $M(z=0)$). Let $T(z) \equiv Q^{-1}(z)$ denote the matrix of right eigenvectors of $M(z)$ and write

$$T = \begin{pmatrix} T^{\mathrm{I}} & T^{\mathrm{II}} \end{pmatrix},$$

where T^{I} has dimension $n \times l$ and T^{II} has dimension $n \times (n-l)$. In terms of the characteristic variable $f = T^{-1}\hat{u}$, the boundary conditions become

$$\begin{aligned} E^{\mathrm{I}}Tf &= 0, \qquad \text{at } x = 0 \\ E^{\mathrm{II}}Tf &= 0, \qquad \text{at } x = L. \end{aligned}$$

At $x = 0$, the boundary condition may then be written

$$E^{\mathrm{I}} \begin{pmatrix} T^{\mathrm{I}} & T^{\mathrm{II}} \end{pmatrix} \begin{pmatrix} f^{\mathrm{I}} \\ f^{\mathrm{II}} \end{pmatrix} = 0, \qquad \text{i.e., } C^{\mathrm{I}} f^{\mathrm{I}} + D^{\mathrm{I}} f^{\mathrm{II}} = 0,$$

where $C^{\mathrm{I}} := E^{\mathrm{I}} T^{\mathrm{I}}$ is an $l \times l$ matrix, and $D^{\mathrm{I}} := E^{\mathrm{I}} T^{\mathrm{II}}$ is an $l \times (n-l)$ matrix. Recall that the f^{I} modes are purely rightgoing and the f^{II} modes are purely leftgoing, so here we may solve for the incoming (rightgoing) modes as long as C^{I} is nonsingular. In that case,

$$f^{\mathrm{I}} = -\left(C^{\mathrm{I}}\right)^{-1} D^{\mathrm{I}} f^{\mathrm{II}} = R^{\mathrm{I}} f^{\mathrm{II}},$$

where the $l \times (n-l)$ matrix R^{I} is the matrix of reflection coefficients.

Similarly, at the right boundary the boundary condition may be written

$$D^{\mathrm{II}} f^{\mathrm{I}} + C^{\mathrm{II}} f^{\mathrm{II}} = 0,$$

where $C^{\mathrm{II}} := E^{\mathrm{II}} T^{\mathrm{II}}$ has dimension $(n-l) \times (n-l)$, and $D^{\mathrm{II}} := E^{\mathrm{II}} T^{\mathrm{I}}$ has dimension $(n-l) \times l$. Here we may solve for the incoming (leftgoing) modes if C^{II} is nonsingular, in which case

$$f^{\mathrm{II}} = -\left(C^{\mathrm{II}}\right)^{-1} D^{\mathrm{II}} f^{\mathrm{I}} = R^{\mathrm{II}} f^{\mathrm{I}},$$

where R^{II} is the $(n-l) \times l$ matrix of reflection coefficients at the right boundary.

For a pair of boundary conditions to be perfectly nonreflecting, the matrices R^{I} and R^{II} must be identically zero, so the matrices D^{I} and D^{II} must be zero. Taking E^{I} and E^{II} equal to the left eigenvectors Q^{I} and Q^{II} not only makes the $D^{\mathrm{I,II}}$ matrices zero, but also makes the $C^{\mathrm{I,II}}$ matrices diagonal. Thus, in order to construct a perfectly nonreflecting boundary condition it is *sufficient* to use the left eigenvectors (as long as the boundary condition is well posed), but it is not necessary. Equivalently, it is not necessary that the matrix

$$C = \begin{pmatrix} C^{\mathrm{I}} & D^{\mathrm{I}} \\ D^{\mathrm{II}} & C^{\mathrm{II}} \end{pmatrix}$$

be diagonal; it is only necessary that it be *block* diagonal.

In order to solve for the incoming modes in terms of the outgoing modes, we required at the right boundary that the matrix C^{I} be nonsingular, and at the left boundary that C^{II} be nonsingular. This requirement is equivalent to the uniform Kreiss condition [11, 14, 18], which is a sufficient condition for well-posedness, but it is more strict than necessary. As discussed in [14], for well-posedness all we really require is that the reflection coefficient matrices R^{I} and R^{II} be bounded for all $z \in \mathbb{C}$, a requirement that is equivalent to the well-posedness criteria described by Giles [7].

2.2. *Application to Euler Equations*

In this section we derive continuous nonreflecting boundary conditions for the Euler equations of gas dynamics. The standard procedure, as described in the previous section, is to construct the matrix $M(z)$, determine which modes are incoming by looking at the eigenvalues of $M(0)$, and then to write down the appropriate nonreflecting boundary condition from the left eigenvectors of M that correspond to incoming modes.

The linearized Euler equations are a particularly difficult example, because the exact boundary conditions are nonlocal, and all local boundary conditions obtained by approximating the left eigenvectors by rational functions are ill posed, as we discuss in Subsection 2.2.3.

2.2.1. Equations of motion. The isentropic Euler equations of gas dynamics, linearized about a uniform base flow, may be written

$$\begin{aligned} u_t + Uu_x + Vu_y + p_x &= 0 \\ v_t + Uv_x + Vv_y + p_y &= 0 \\ p_t + Up_x + Vp_y + u_x + v_y &= 0, \end{aligned} \tag{2.6}$$

where U and V are the Mach numbers of the uniform base flow in the x and y directions. Here, the velocities u and v are normalized with respect to the (constant) sound speed, and the pressure p is normalized by the ambient density times the sound speed squared. Lengths are made dimensionless with an (as yet unspecified) length L, and time is made dimensionless with L and the sound speed. In matrix form, with $w = (u, v, p)^T$, we have

$$w_t + \tilde{A}w_x + \tilde{B}w_y = 0,$$

where

$$\tilde{A} = \begin{pmatrix} U & 0 & 1 \\ 0 & U & 0 \\ 1 & 0 & U \end{pmatrix}, \qquad \tilde{B} = \begin{pmatrix} V & 0 & 0 \\ 0 & V & 1 \\ 0 & 1 & V \end{pmatrix}$$

so the system (2.6) is symmetric hyperbolic, and hence strongly hyperbolic. It is convenient to diagonalize the matrix $\tilde{A}$ by transforming the equations to the variables $q = (v, u + p, u - p)$. The system becomes

$$q_t + Aq_x + Bq_y = 0, \tag{2.7}$$

where

$$A = \begin{pmatrix} U & 0 & 0 \\ 0 & U+1 & 0 \\ 0 & 0 & U-1 \end{pmatrix}, \qquad B = \begin{pmatrix} V & 1/2 & -1/2 \\ 1 & V & 0 \\ -1 & 0 & V \end{pmatrix}.$$

Here we assume $0 < U < 1$ (subsonic flow), so the matrix A is invertible, and we may construct the matrix $M(z) = A^{-1}(I + zB)$ as in the previous section. Taking a Fourier transform in y and a Laplace transform in time, with (ik, s) the dual variables of (y, t), the equations of motion become

$$\hat{q}_x = -\tilde{s}M(z)\hat{q}, \tag{2.8}$$

where $\tilde{s} = s + ikV$, $z = ik/\tilde{s}$, and

$$M(z) = \begin{pmatrix} \frac{1}{U} & \frac{z}{2U} & \frac{-z}{2U} \\ \frac{z}{U+1} & \frac{1}{U+1} & 0 \\ \frac{-z}{U-1} & 0 & \frac{1}{U-1} \end{pmatrix}. \tag{2.9}$$

2.2.2. Exact nonlocal boundary conditions. The direction of propagation of the modes is determined from the eigenvalues of $M(z)$, which are

$$\begin{aligned}\lambda_1 &= \frac{1}{U}\\ \lambda_2 &= \frac{U-\gamma}{U^2-1}\\ \lambda_3 &= \frac{U+\gamma}{U^2-1},\end{aligned}$$

where $\gamma(z)=\sqrt{1-z^2(1-U^2)}$, and where $\sqrt{\cdot}$ denotes the standard branch of the square root. Since $0<U<1$, the first two modes are rightgoing ($\lambda_1, \lambda_2 > 0$ for $z=0$), and the third mode is leftgoing ($\lambda_3<0$ for $z=0$).

We stated earlier that approximate boundary conditions give the highest error for waves that are tangent to the boundary. Let us identify these waves for the linearized Euler equations. The x-components of the group velocities of the modes are

$$\begin{aligned}c_{g_1} &= U\\ c_{g_2} &= \frac{U^2-1}{U-1/\gamma}\\ c_{g_3} &= \frac{U^2-1}{U+1/\gamma}.\end{aligned}$$

Waves are tangent to the boundary when the x-component of the group velocity is zero, so the last two modes (the acoustic waves) are tangent to the boundary when $\gamma=0$.

The boundary conditions are found from the left eigenvectors of $M(z)$, which are the rows of the matrix

$$Q(z)=\left(\frac{Q^{\mathrm{I}}}{Q^{\mathrm{II}}}\right)=\left(\begin{array}{ccc}2 & z(U+1) & z(U-1)\\ -2zU & 1+\gamma & 1-\gamma\\ \hline -2zU & 1-\gamma & 1+\gamma\end{array}\right) \tag{2.10}$$

partitioned into Q^{I} and Q^{II} as shown. At the left boundary ($x=0$), the appropriate nonreflecting boundary condition is then

$$Q^{\mathrm{I}}\hat{q}=0, \qquad \text{i.e.,} \begin{pmatrix}2 & z(U+1) & z(U-1)\\ -2zU & 1+\gamma & 1-\gamma\end{pmatrix}\begin{pmatrix}\hat{v}\\ \hat{u}+\hat{p}\\ \hat{u}-\hat{p}\end{pmatrix}=0 \tag{2.11}$$

and at the right boundary ($x=L$), the nonreflecting boundary condition is

$$Q^{\mathrm{II}}\hat{q}=0, \qquad \text{i.e.,} \begin{pmatrix}-2zU & 1-\gamma & 1+\gamma\end{pmatrix}\begin{pmatrix}\hat{v}\\ \hat{u}+\hat{p}\\ \hat{u}-\hat{p}\end{pmatrix}=0. \tag{2.12}$$

These conditions are exact, but they are nonlocal, since γ is not a rational function of z. Furthermore, when γ is approximated by a rational function, the "inflow" boundary condition (2.11) is always ill posed, as we will show in the next section.

2.2.3. Well-posed local approximations. Before discussing local approximations to the above boundary conditions, and in particular their well-posedness, we require some background on approximation by rational functions. In order to develop well-posed one-way boundary conditions for the scalar wave equation, Trefethen and Halpern [27] proved several theorems about rational approximations of $\sqrt{1-z^2}$. In particular, they proved that if $r_0(z)$ is a rational function that approximates $\sqrt{1-z^2}$ for $z \in [-1, 1]$, then as long as $r_0(z)$ interpolates $\sqrt{1-z^2}$ at sufficiently many points in the interval $(-1, 1)$, the equation

$$r_0(z) = -\sqrt{1-z^2} \tag{2.13}$$

has no solutions. The existence of solutions of (2.13) is directly relevant in showing well-posedness of approximate boundary conditions. Conveniently, the interpolation criteria mentioned are met for many common categories of approximations. In particular, if $r_0(z)$ is of degree (m, n) (i.e., the numerator and denominator are polynomials of degree m and n, respectively), and $r_0(z)$ is a Padé, Chebyshev, or least-squares approximation to the square root, the interpolation criteria are met as long as $m = n$ or $m = n + 2$.

Now, to obtain local approximations to the exact nonreflecting boundary conditions derived in the previous section, we replace $\gamma(z) = \sqrt{1 - z^2(1-U^2)}$ in the boundary conditions (2.11) and (2.12) by a rational function $r(z) = r_0(z\sqrt{1-U^2})$, where r_0 meets the interpolation criteria mentioned above. To find the reflection coefficients, as in Subsection 2.1, we require the matrix of right eigenvectors of $M(z)$, given by

$$T(z) = \left(T^{\mathrm{I}} \mid T^{\mathrm{II}}\right) = \left(\begin{array}{cc|c} 1 & -z & -z \\ zU & \frac{1+\gamma}{U+1} & \frac{1-\gamma}{U+1} \\ zU & \frac{1-\gamma}{U-1} & \frac{1+\gamma}{U-1} \end{array}\right)$$

partitioned as shown. Computing the matrices of reflection coefficients as described in Subsection 2.1, at the right boundary we find

$$R^{\mathrm{II}} = -\left(Q^{\mathrm{II}}T^{\mathrm{II}}\right)^{-1} Q^{\mathrm{II}}T^{\mathrm{I}} = \begin{pmatrix} 0 & R_2 \end{pmatrix},$$

where

$$R_2 = \frac{(\gamma - r)(\gamma U - 1)}{(\gamma + r)(\gamma U + 1)}. \tag{2.14}$$

Now, for well-posedness, we require R_2 be bounded. Clearly, the second factor in the denominator is never zero, since whenever γ is real, γ is positive. Additionally, the first factor in the denominator is never zero, as guaranteed by the theorem of Trefethen and Halpern. Thus the right boundary condition is well posed. Note, however, that for waves tangent to the boundary ($\gamma = 0$), the reflection coefficient is always unity, independent of the rational function approximation r.

At the left boundary, the reflection coefficient matrix is

$$R^{\mathrm{I}} = -\left(Q^{\mathrm{I}}T^{\mathrm{I}}\right)^{-1} Q^{\mathrm{I}}T^{\mathrm{II}} = \begin{pmatrix} 0 \\ R_1 \end{pmatrix},$$

where

$$R_1 = -\frac{(\gamma - r)(\gamma U + 1)}{(\gamma + r)(\gamma U - 1)}. \tag{2.15}$$

Here, as before, the first factor in the denominator is never zero, but the second factor is zero when $z^2 = -1/U^2$. Since the reflection coefficient is unbounded for this value of z, the left boundary condition is ill posed, regardless of how we choose the approximation $r(z)$. To obtain a well-posed approximate boundary condition, we must modify the exact boundary condition given by (2.11).

The modified inflow boundary condition. Recall that the only requirement for a boundary condition $E^{\mathrm{I}}q = 0$ to be perfectly nonreflecting is that $E^{\mathrm{I}}T^{\mathrm{II}} = 0$, or physically, that all purely outgoing modes identically satisfy the boundary condition. Here, at the left boundary there is only one outgoing mode—the matrix T^{II} is a single column vector, which we denote e_3—so all we require is that the rows of E^{I} be orthogonal to e_3. The matrix Q of left eigenvectors provides two such rows, given by (2.11), but these row vectors are linearly dependent for $z^2 = -1/U^2$, and so the resulting boundary condition is ill posed. We need another way to come up with row vectors orthogonal to e_3.

One way, proposed by Goodrich and Hagstrom [8], is to consider the matrix $M - \lambda_3 I$. By definition of e_3,

$$(M - \lambda_3 I)e_3 = 0$$

so each row of $M - \lambda_3 I$ is a row vector orthogonal to e_3. For our case,

$$M - \lambda_3 I = \begin{pmatrix} \frac{\gamma U+1}{U(1-U^2)} & \frac{z}{2U} & \frac{-z}{2U} \\ \frac{z}{1+U} & \frac{\gamma+1}{1-U^2} & 0 \\ \frac{z}{1-U} & 0 & \frac{\gamma-1}{1-U^2} \end{pmatrix}. \tag{2.16}$$

Goodrich and Hagstrom take the second row of this matrix, scaled by the constant $1 - U^2$, in place of the second row of Q^{I}, to give the pair of boundary conditions

$$\begin{aligned} E^{\mathrm{I}}\hat{q} &= 0, \qquad \text{at } x = 0 \\ E^{\mathrm{II}}\hat{q} &= 0, \qquad \text{at } x = L, \end{aligned} \tag{2.17}$$

where

$$\begin{aligned} E^{\mathrm{I}} &= \begin{pmatrix} 2 & z(U+1) & z(U-1) \\ z(1-U) & 1+r & 0 \end{pmatrix} \\ E^{\mathrm{II}} &= \begin{pmatrix} -2zU & 1-r & 1+r \end{pmatrix}, \end{aligned} \tag{2.18}$$

where again we have replaced γ with its rational function approximation r. The right boundary condition is the same as before, but now the reflection coefficient at the left boundary is

$$R_1 = -\frac{(\gamma - r)(\gamma - 1)}{(\gamma + r)(\gamma + 1)} \tag{2.19}$$

which has no poles, and so this boundary condition is well posed. Here again, note that waves tangent to the boundary are perfectly reflected, regardless of the approximation r.

Other approximations. It is interesting to take an arbitrary linear combination of rows of $M - \lambda_3 I$ in place of the second row of Q^{I}. Denoting the three rows of $M - \lambda_3 I$ as x_1, x_2, and x_3, respectively (where the x_j are row vectors), and choosing a linear combination of them $a_1x_1 + a_2x_2 + a_3x_3$ in place of the second row of Q gives the reflection coefficient

$$R_1 = -\left(\frac{\gamma - r}{\gamma + r}\right)\left(\frac{a_1 z + a_2(\gamma - 1)/(1 + U) + a_3(\gamma + 1)/(1 - U)}{-a_1 z + a_2(\gamma + 1)/(1 + U) + a_3(\gamma - 1)/(1 - U)}\right). \tag{2.20}$$

From this expression, several points are evident. First, using the third row of $M - \lambda_3 I$ (i.e., taking $a_1 = a_2 = 0$, $a_3 = 1$) gives an ill-posed boundary condition, because of the factor $(\gamma - 1)$ in the denominator. Second, using the first row ($a_1 = 1$, $a_2 = a_3 = 0$) gives a reflection coefficient $(\gamma - r)/(\gamma + r)$, which is greater in magnitude than (2.19) for all waves. Thus, the second row is the most sensible choice. It is possible to make the reflection coefficient even smaller than (2.19), by choosing

$$\begin{aligned} a_1 &= 0 \\ a_2 &= (r + 1)(U + 1) \\ a_3 &= (r - 1)(U - 1) \end{aligned}$$

in which case the reflection coefficient (2.20) becomes

$$R_1 = -\left(\frac{\gamma - r}{\gamma + r}\right)^2 \tag{2.21}$$

which approaches zero even faster than (2.19) as $r \to \gamma$. However, the corresponding row of the matrix E^{I}

$$\begin{pmatrix} 2z & \dfrac{(r + 1)^2}{1 - U} & -\dfrac{(r - 1)^2}{1 + U} \end{pmatrix} \tag{2.22}$$

contains r^2 terms. Thus, while this boundary condition is more accurate than the one given by (2.17) and (2.18), it also requires more computational effort. In fact, for the same computational effort we may double the degree of the rational function approximation r in (2.18) and obtain an even better reflection coefficient. Thus, in what follows we consider the boundary condition given by (2.17) and (2.18), but note that it may be possible to obtain better reflection coefficients for other choices of a_1, a_2, and a_3.

2.2.4. Comparison with previous boundary conditions. Goodrich and Hagstrom [8] implement the boundary condition given in the previous section using a particular approximation to γ. Their local approximation to γ is identical to the (4,4) Padé approximation, though this is not immediately obvious, because the approximation was derived using a different approach (approximating a pseudo-differential operator via quadrature) and is expressed in [12] in terms of partial fractions. We note that the earlier boundary conditions described by Hagstrom in [12] are actually ill posed at the inflow since these use the matrix of left eigenvectors Q, from (2.10). Thus his nonlocal approximations to γ (which have excellent bounds on long-time errors) should presumably be applied in conjunction with (2.17).

It is of interest to compare the present results with the boundary conditions of Giles [7], which have been widely used in compressible flow and aeroacoustic calculations.

Giles [7] provides two boundary conditions. His standard boundary conditions use the left eigenvectors, with the approximation $\gamma \approx 1$. Thus, the standard inflow boundary condition is ill posed, as discussed in the previous section, and the outgoing reflection coefficient is given by (2.14), with $r = 1$, which gives

$$R^{\mathrm{II}} = \begin{pmatrix} 0 & -\dfrac{(\gamma-1)(\gamma U-1)}{(\gamma+1)(\gamma U+1)} \end{pmatrix} = \begin{pmatrix} 0 & O(z^2) \end{pmatrix} \qquad \text{as } z \to 0.$$

His modified boundary conditions are given by the matrix

$$E = \left(\begin{array}{ccc} 2 & z(U+1) & z(U-1) \\ z(1-U) & 2 & 0 \\ \hline -z(1+U) & 0 & 2 \end{array}\right)$$

with reflection coefficients

$$R^{\mathrm{I}} = \begin{pmatrix} 0 \\ -\frac{(\gamma-1)^2}{(\gamma+1)^2} \end{pmatrix} = \begin{pmatrix} 0 \\ O(z^4) \end{pmatrix} \qquad \text{as } z \to 0$$

and

$$R^{\mathrm{II}} = \begin{pmatrix} -\dfrac{z(1-U)^2}{(\gamma+1)^2} & -\dfrac{(\gamma-1)^2}{(\gamma+1)^2} \end{pmatrix} = \begin{pmatrix} O(z) & O(z^4) \end{pmatrix} \qquad \text{as } z \to 0.$$

(Note that the reflection coefficients given in [7] differ by constant factors from the ones given here, because Giles normalizes the right eigenvectors differently.)

For comparison with the boundary conditions presented here, if r is a Padé approximation of degree (m, n), as $z \to 0$ our reflection coefficients are

$$R^{\mathrm{I}} = \begin{pmatrix} 0 \\ O(z^{m+n+4}) \end{pmatrix}$$

and

$$R^{\mathrm{II}} = \begin{pmatrix} 0 & O(z^{m+n+2}) \end{pmatrix}.$$

3. DISCRETELY NONREFLECTING BOUNDARY CONDITIONS

If the nonreflecting boundary conditions discussed in the previous section are to be used in conjunction with a finite-difference method for solving the system (2.1), the boundary conditions must be discretized and combined with finite-difference equations for the interior points. Typically, details of this implementation have not been discussed in the literature. Often implementation involves ad hoc boundary closures for finite-difference schemes (one-sided schemes at the boundaries, and special schemes for near boundary nodes when large stencil interior schemes are used). Some specific schemes have been presented for compact finite-difference schemes [19], and for dispersion-relation preserving (DRP) schemes [23]. However, a detailed analysis of accuracy and stability of these schemes has not been carried

out when they are applied to various boundary conditions. In a more rigorous treatment, Carpenter *et al.* [2] have proposed particular boundary closures for high-order finite-difference approximations to one-dimensional hyperbolic systems. These schemes are constructed to couple physical boundary conditions to the boundary closure of the finite-difference scheme and can be proven to be stable. However, the boundary conditions they use do not account for the dispersive nature of the finite-difference scheme and do not attempt to control the extent to which spurious waves are reflected by smooth waves.

Spurious waves, which will be formally defined in Subsection 3.1, are an artifact of the discretization, and have been extensively analyzed by Vichnevetsky [29] for the one-dimensional advection equation. In a previous paper [3], we showed how to develop closures for both downstream and upstream boundaries of the simple advection equation. These boundary conditions maintain the desired order of accuracy of the interior scheme, are stable, and minimize reflection of smooth and spurious waves at artificial boundaries. The closure for the "downstream" boundary of the simple advection equation is similar to a closure of the finite-difference scheme, at least up through the order of accuracy of the interior scheme. "Upwind" boundary closures, however, are not derivative operators but instead are designed to eliminate any reflection of upstream-propagating spurious waves. The hierarchy of upwind conditions contains, as a special case, the upwind boundary conditions developed by Vichnevetsky [29].

We first review this previous work on the simple advection equation, and in Subsection 3.2 we extend the methodology to obtain numerically nonreflecting boundary conditions for a system of one-dimensional equations in which all solutions to the continuous equations propagate in the same direction (*one-way* equations). We then show in Subsection 3.3 how these results may be applied directly to two-dimensional equations of the form (2.1), again so long as all the physical modes travel in the same direction. An example of such a problem is the Euler equations linearized about a supersonic mean flow. Finally, in Subsection 3.4 we treat the more general *two-way* equations of the form (2.1), such as the Euler equations linearized about a subsonic mean flow. The general procedure is to use the continuous boundary conditions of Section 2 to split the system into two one-way equations, and then apply the discrete boundary conditions of Subsection 3.3 to each one-way system.

3.1. *Finite Difference Schemes and Spurious Waves*

Several artifacts of finite difference approximations to hyperbolic equations play prominent roles in the development of accurate and robust artificial boundary conditions. In this section we introduce these phenomena in the context of the simple scalar advection equation in one dimension

$$u_t + u_x = 0 \tag{3.1}$$

which admits solutions of the form

$$u(x, t) = \mathrm{e}^{i(kx-\omega t)}. \tag{3.2}$$

Inserting (3.2) into (3.1) gives the dispersion relation $\omega = k$, so for this example the phase velocity ($c_p = \omega/k$) and group velocity ($c_g = d\omega/dk$) both equal 1.

We are interested in how discretization affects the above dispersion relation. We restrict our attention to the family of three-point central finite difference schemes given by

$$\alpha(u_x)_{j+1} + (u_x)_j + \alpha(u_x)_{j-1} = \frac{a}{h}(u_{j+1} - u_{j-1}), \tag{3.3}$$

where we have introduced a uniform grid in x, with mesh spacing h, and where $u_j(t)$ denotes the approximation to $u(jh, t)$. See [19] for a detailed discussion of compact difference schemes. For our purposes, it suffices to note that if $\alpha = 0$ and $a = 1/2$, we recover the standard second-order central difference scheme discussed above, and if $\alpha = 1/4$ and $a = 3/4$, we obtain the fourth-order Padé scheme. The extension to wider stencils is discussed briefly below.

In this paper we consider exclusively a semi-discrete scheme, and hence neglect dispersive and dissipative effects of time discretization. Vichnevetsky [29] has shown that the energy reflected at a boundary is invariant under time discretization and is equal to the energy reflected in the semi-discrete case. Moreover, in cases when the semi-discrete equation is solved with a 4th-order Runge–Kutta method, it has been shown in the one-dimensional case that the additional dispersion and dissipation are essentially negligible for CFL numbers smaller than one (see [3]).

For the schemes given by (3.3), the modified wavenumber is

$$\tilde{k}h = \frac{2a \sin kh}{1 + 2\alpha \cos kh}.$$

Figure 1 shows the dispersion relation $\omega = \tilde{k}$ and group velocity for the second- and fourth-order schemes applied to the scalar advection equation (3.1).

Note that well-resolved waves ($kh \ll 1$) travel with approximately the same group velocity as solutions of the continuous equation, but poorly resolved waves (increasing kh) travel with unphysical group velocities, and the most poorly resolved waves ($kh \approx \pi$) travel in the opposite direction. These waves that travel in the wrong direction have been called *spurious numerical waves*, after Vichnevetsky [29].

Finally, note that for each frequency ω (below some critical value ω_c), there corresponds *two* values of k that satisfy the dispersion relation: a "physical" solution which travels in the correct direction ($c_g > 0$), and a "spurious" solution which travels in the opposite direction ($c_g < 0$), while for the continuous equation there was only one wavenumber k for each

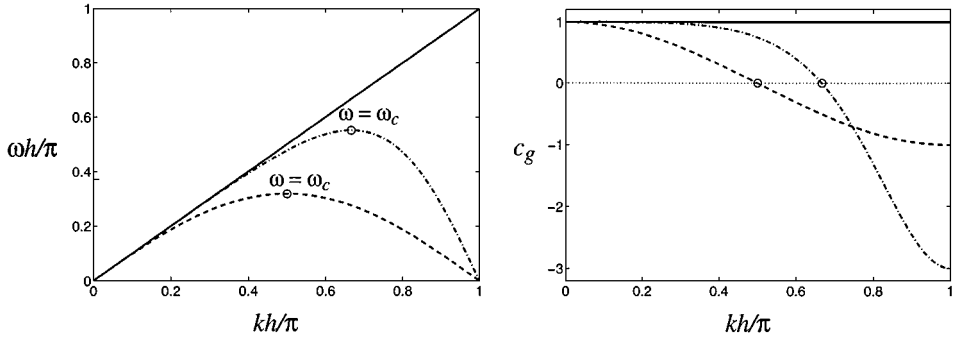

FIG. 1. Dispersion relation for the simple advection equation, with exact derivative, —; second-order central difference scheme, - - -; and fourth-order Padé method, - · -; and corresponding group velocity for the same schemes.

frequency ω. The two numerical solutions are uncoupled in the interior, but are (usually) coupled by the boundary conditions. Even in the simple one-way advection equation, physical waves reflect as spurious waves at the downwind boundary, with the opposite reflection at the upwind boundary.

Difference approximations with larger stencils than (3.3) will have more than one spurious solution, though additional solutions will be spatially damped. If we wish to develop nonreflecting boundary conditions, we must consider how all of the physical and spurious solutions are coupled at the boundary and attempt to minimize any reflections. For larger stencils, the algebra becomes significantly more complicated. In order to concisely demonstrate the procedure, we restrict our attention here to the 3-point stencil.

3.2. *One-Dimensional Numerical Boundary Conditions*

Here we generalize the numerically nonreflecting boundary conditions derived by Colonius [3] for the scalar advection equation

$$u_t + cu_x = 0,$$

where u is a scalar, and apply this methodology to the system of partial differential equations

$$u_x = -Mu_t \tag{3.4}$$

for $0 < x < L$, where u is a vector with n components, and M is an $n \times n$ positive-definite matrix. Although the matrix M is diagonalizable, here we shall not exploit this property, as this in general is not the case for problems beyond one dimension. The following analysis is readily applicable to the multidimensional case, addressed in Subsections 3.3–3.4.

Separation of spurious and physical modes. Let us begin by identifying the spurious and physical modes in a finite-difference approximation to (3.4). Introduce a regular grid in x, with mesh spacing h, and let u_k denote the approximation to $u(x = kh)$. Applying the family of three-point finite difference schemes mentioned in the previous section to (3.4) gives

$$\alpha(-Mu_t)_{k+1} + (-Mu_t)_k + \alpha(-Mu_t)_{k-1} = \frac{a}{h}(u_{k+1} - u_{k-1}). \tag{3.5}$$

Now introduce a (normal mode) solution of the form

$$u_k(t) = \hat{u}\, \mathrm{e}^{i\omega t}\kappa^k, \tag{3.6}$$

where $\hat{u} \in \mathbb{R}^n$, $\omega \in \mathbb{R}$, and $\kappa \in \mathbb{C}$, so that

$$u_{k+1} = \kappa\, u_k \tag{3.7}$$

and (3.5) becomes

$$\left[\kappa^2(aI + \alpha i\omega hM) + \kappa(i\omega hM) - (aI - \alpha i\omega hM)\right]\hat{u} = N(i\omega, \kappa)\hat{u} = 0, \tag{3.8}$$

where $N(i\omega, \kappa)$ is the matrix in brackets. This linear system has nontrivial solutions only when

$$\det N(i\omega, \kappa) = 0. \tag{3.9}$$

Equation (3.9) is the dispersion relation for the discretized system. Without loss of generality we may assume the matrix M is in Jordan form (similarity transform Eq. (3.8)), and so

$$\det N(i\omega,\kappa)=\prod_{j=1}^{n}\left[\kappa^2(a+\alpha i\omega h\lambda_j)+\kappa(i\omega h\lambda_j)-(a-\alpha i\omega h\lambda_j)\right],$$

where the λ_j $(j=1,\ldots,n)$ are eigenvalues of M. Defining

$$\phi_j=\omega h\lambda_j,\qquad \text{for } j=1,\ldots,n$$

and solving (3.9) for κ gives

$$\kappa^{\pm j}=\frac{-i\phi_j\pm\sqrt{4a^2-\phi_j^2(1-4\alpha^2)}}{2(a+\alpha i\phi_j)},\tag{3.10}$$

where the $\kappa^{\pm j}$ satisfy

$$(\kappa^{\pm j})^2(a+\alpha i\phi_j)+\kappa^{\pm j}i\phi_j-(a-\alpha i\phi_j)=0$$

for all $j=1,\ldots,n$. Solutions are waves when $|\kappa|=1$, which corresponds to $|\phi_j|\le\phi_c$, where $\phi_c=2a/\sqrt{1-4\alpha^2}$. Note that the number of roots (3.10) of the dispersion relation for the discretized equations is $2n$, while the dispersion relation of the non-discretized system has only n roots, corresponding to the n eigenvalues of M. Here, the κ^+ roots correspond to the "physical" solutions, and the κ^- roots correspond to the "spurious" modes mentioned in the previous section. Higher order difference schemes will have additional spurious modes.

To distinguish the physical parts of the solution from the spurious parts, we consider a solution that is a superposition of modes of the form (3.6) and write the solution u_k at any grid point k as

$$u_k=\sum_{j=1}^{n}\left(u_k^{+j}+u_k^{-j}\right),$$

where the $u_k^{\pm j}$ are normal modes of the form (3.6) that satisfy

$$N(i\omega,\kappa^{\pm j})u_k^{\pm j}=0$$

for all $j=1,\ldots,n$. Note that

$$u_{k+1}^{\pm j}=\kappa^{\pm j}u_k^{\pm j}.$$

Exact nonreflecting boundary conditions. The exact nonreflecting boundary condition at the left boundary ($k=0$) is $u_0^{+j}=0$ for $j=1,\ldots,n$. This is equivalent to

$$u_0^j=\frac{1}{\kappa^{-j}}u_1^j,\qquad \text{for all } j=1,\ldots,n\tag{3.11}$$

since (3.11) may be written

$$\begin{aligned} u_0^{+j} + u_0^{-j} &= \frac{1}{\kappa^{-j}}\left(u_1^{+j} + u_1^{-j}\right) \\ \Leftrightarrow\ u_0^{+j} + u_0^{-j} &= \frac{\kappa^{+j}}{\kappa^{-j}} u_0^{+j} + u_0^{-j} \\ \Leftrightarrow\ \left(1 - \frac{\kappa^{+j}}{\kappa^{-j}}\right) u_0^{+j} &= 0 \\ \Leftrightarrow\ u_0^{+j} &= 0 \end{aligned}$$

since $\kappa^{+j} \neq \kappa^{-j}$ (unless $\phi = \phi_c$). Similarly, the exact nonreflecting boundary condition at the right boundary ($k = N$) may be written

$$u_N^j = \kappa^{+j} u_{N-1}^j. \tag{3.12}$$

Because the $\kappa^{\pm j}$, given by (3.10), are not rational functions of the frequency ω, when the boundary conditions (3.11) and (3.12) are transformed back into physical space they will be nonlocal in time, as mentioned earlier. We wish to derive approximate nonreflecting boundary conditions that are local in space and time.

Approximate nonreflecting boundary conditions. After Colonius [3], we consider a numerical boundary condition at the left boundary ($k = 0$) in the form of a closure for the x-derivative. That is, we seek an approximately nonreflecting boundary condition of the form

$$M \frac{\mathrm{d}u_0}{\mathrm{d}t} = \frac{1}{c_1 h} \sum_{k=0}^{N_d} d_k u_k,$$

where c_1 and $d_k (k = 0, \ldots, N_d)$ are coefficients to be determined and M is still the matrix from (3.4). Taking a Fourier transform in time and splitting u into its rightgoing and leftgoing modes, the boundary condition becomes

$$c_1 i\omega h M \sum_{j=1}^{n} \left(u_0^{+j} + u_0^{-j}\right) = \sum_{k=0}^{N_d} d_k \left(\sum_{j=1}^{n} \left(u_k^{+j} + u_k^{-j}\right) \right) \tag{3.13}$$

$$\Leftrightarrow \sum_{j=1}^{n} \left(c_1 i\omega h M u_0^{+j} - \sum_{k=0}^{N_d} d_k (\kappa^{+j})^k u_0^{+j} \right) = \sum_{j=1}^{n} \left(- c_1 i\omega h M u_0^{-j} + \sum_{k=0}^{N_d} d_k (\kappa^{-j})^k u_0^{-j} \right). \tag{3.14}$$

Now, it is shown in the Appendix that

$$N(i\omega, \kappa^{\pm j}) u = 0 \Leftrightarrow Mu = \lambda_j u. \tag{3.15}$$

Hence,

$$M u^{\pm j} = \lambda_j u^{\pm j}, \qquad j = 1, \ldots, n$$

and so, writing $\phi_j = \omega h \lambda_j$, and recalling from (3.10) that for a particular scheme $\kappa^{\pm j}$ is a function only of ϕ_j, (3.14) becomes

$$\sum_{j=1}^{n} c(\phi_j) u_0^{+j} = \sum_{j=1}^{n} d(\phi_j) u_0^{-j}, \tag{3.16}$$

where

$$\begin{aligned} c(\phi_j) &= c_1 i \phi_j - \sum_{k=0}^{N_d} d_k (\kappa^{+j})^k \\ d(\phi_j) &= -c_1 i \phi_j + \sum_{k=0}^{N_d} d_k (\kappa^{-j})^k. \end{aligned} \tag{3.17}$$

Now for the boundary condition to be exact ($u_0^{+j} = 0, \forall j$), we require $d(\phi) = 0$, and for the boundary condition to be well-posed we require $d(\phi)/c(\phi)$ be bounded. So, we pick the coefficients c_1 and d_k in order to minimize $d(\phi)$ in some sense. Here, we consider the Taylor series of $d(\phi)$ about $\phi = 0$ and choose the coefficients so that as many terms as possible in the Taylor series are zero. Note that ϕ is proportional to h, and thus a Taylor series expansion about $\phi = 0$ is consistent with the convergence of the discrete approximation in the limit as $h \to 0$. The resulting errors (and reflections) are $O(\phi^{N_d+1})$ as $\phi \to 0$. Well-posed schemes of various orders were derived in [3]; some of these are repeated for convenience in Table I. (The column labeled bc0 is an ad hoc boundary condition which will be discussed in Section 4.) Apparently, stable schemes to arbitrarily high order can be determined (see [3]).

The right boundary condition is treated similarly. For the point u_N we start with

$$a_1 h M \frac{\mathrm{d}u_N}{\mathrm{d}t} = \sum_{k=0}^{N_b} b_k u_{N-k},$$

where a_1 and b_k ($k = 0, \ldots, N_b$) are coefficients to be determined. Separating the spurious and physical modes, as above, gives

$$\sum_{j=1}^{n} a(\phi_j) u_N^{+j} = \sum_{j=1}^{n} b(\phi_j) u_N^{-j} \tag{3.18}$$

where

$$\begin{aligned} a(\phi_j) &= a_1 i \phi_j - \sum_{k=0}^{N_b} \frac{b_k}{(\kappa^{+j})^k} \\ b(\phi_j) &= -a_1 i \phi_j + \sum_{k=0}^{N_b} \frac{b_k}{(\kappa^{-j})^k}. \end{aligned} \tag{3.19}$$

Here, for the boundary condition to be exact ($u_N^{-j} = 0, \forall j$), we require $a(\phi) = 0$, while

TABLE I
Coefficients for Numerically Nonreflecting Boundary Conditions, with the Interior Scheme $a = 3/4$, $\alpha = 1/4$

Scheme	bc0	bc1	bc2	bc4	bc6	bc8
Order	—	2	3	5	7	9
a_1		1	2	12	72	432
b_0		−1	−3	−25	−175	−1143
b_1		1	4	48	424	3236
b_2			−1	−36	−521	−5366
b_3				16	456	6852
b_4				−3	−253	−6208
b_5					80	3868
b_6					−11	−1578
b_7						380
b_8						−41
c_1	1	−1	−2	−4	−8	−16
d_0	0	3	9	45	189	747
d_1		3	12	120	792	4380
d_2			3	132	1539	12318
d_3				72	1704	20796
d_4				15	1095	22560
d_5					384	15972
d_6					57	7170
d_7						1860
d_8						213

$a(\phi)/b(\phi)$ remains bounded, so we choose the coefficients so that as many terms as possible in the Taylor expansion of $a(\phi)$ are zero. These coefficients are also given in Table I, and for the right boundary condition the reflections are $O(\phi^{N_b+1})$ as $\phi \to 0$. See [3] for a more general treatment of boundary conditions of this type; this reference also demonstrates how to write numerically nonreflecting boundary conditions for boundaries where incoming waves are specified, as in a scattering problem.

For future reference, we introduce a more concise notation for the numerical boundary conditions. At the right boundary, where all physical waves are outgoing, we write the boundary condition as

$$-M\frac{\mathrm{d}u_N}{\mathrm{d}t} = \mathrm{d}_N^o u_N, \tag{3.20}$$

where d_N^o is the operator defined by

$$\mathrm{d}_N^o u_N = -\frac{1}{a_1 h}\sum_{k=0}^{N_b} b_k u_{N-k}. \tag{3.21}$$

At the left boundary, where the physical waves are incoming, the numerical boundary condition is similarly written

$$-M\frac{\mathrm{d}u_0}{\mathrm{d}t} = \mathrm{d}_0^i u_0, \tag{3.22}$$

where d_0^i is defined by

$$\mathrm{d}_0^i u_0 = -\frac{1}{c_1 h} \sum_{k=0}^{N_d} d_k u_k. \tag{3.23}$$

Note that these boundary conditions apply only when M is positive-definite. Similar boundary conditions may also be derived for the case when M is negative-definite, and the coefficients merely change sign. When $M < 0$, physical waves are incoming at the right boundary and outgoing at the left boundary, and the resulting boundary conditions are written

$$-M \frac{\mathrm{d}u_N}{\mathrm{d}t} = \mathrm{d}_N^i u_N \tag{3.24}$$

$$-M \frac{\mathrm{d}u_0}{\mathrm{d}t} = \mathrm{d}_0^o u_0 \tag{3.25}$$

where d_N^i and d_0^o are defined by

$$\mathrm{d}_N^i u_N = \frac{1}{c_1 h} \sum_{k=0}^{N_d} d_k u_{N-k} \tag{3.26}$$

$$\mathrm{d}_0^o u_0 = \frac{1}{a_1 h} \sum_{k=0}^{N_b} b_k u_k. \tag{3.27}$$

Note that with this notation, the boundary conditions given by (3.20), (3.22), (3.24), and (3.25) take the form of the original Eq. (3.4), with the operators $\mathrm{d}_{0,N}^{i,o}$ acting as closures for the x-derivative. So as long as we have a *one-way* equation, we can immediately apply a discrete nonreflecting boundary condition just as easily as applying a closure for a derivative.

3.2.1. Single mode reflection coefficients. The numerical boundary conditions given in Table I are, of course, approximate. One way to quantify the error introduced by the approximation is by means of a reflection coefficient. Take the right boundary first, and consider how a single outgoing mode u^{+j} is reflected. From (3.18), we have

$$\begin{aligned} a(\phi_j) u_N^{+j} &= b(\phi_j) u_N^{-j} \\ \Rightarrow \left\| u_N^{-j} \right\| &= \left| \frac{a(\phi_j)}{b(\phi_j)} \right| \left\| u_N^{+j} \right\| \\ &= \left| \rho^o(\phi_j) \right| \left\| u_N^{+j} \right\|, \end{aligned}$$

where $\rho^o = a/b$ is the numerical reflection coefficient for the outflow boundary condition d^o. It describes the spurious wave reflected by an outgoing physical wave. Similarly, at the left boundary we have

$$\left\| u_0^{+j} \right\| = \left| \rho^i(\phi_j) \right| \left\| u_0^{-j} \right\|,$$

where $\rho^i = d/c$ is the numerical reflection coefficient for the inflow boundary condition d^i, and describes the physical wave reflected by an outgoing spurious wave. The magnitudes of the reflection coefficients are plotted for several choices of coefficients in Fig. 2. Note that waves at the critical frequency always suffer pure reflection.

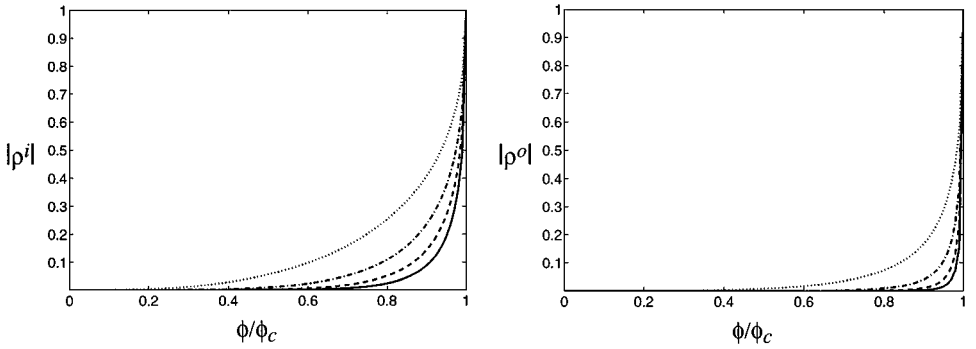

FIG. 2. Inflow and outflow reflection coefficients for boundary conditions bc2, · · ·; bc4, - · -; bc6, - - -; and bc8, —; from Table I.

3.3. *Numerical Boundary Conditions for One-Way Systems*

As before, consider the system

$$u_t + Au_x + Bu_y = 0 \tag{3.28}$$

for $0 < x < L$, $y \in \mathbb{R}$, where u is a vector with n components, and A and B are matrices, but now consider the special case where A is a definite matrix. As described in Section 2, if A is positive-definite, then the n modes of (3.28) all travel to the right, and if A is negative-definite, the modes all travel to the left. Hence, we refer to this special case as a *one-way system*, and for such systems the discrete boundary conditions of Subsection 3.2 may be applied directly.

First, note that it is trivial to write a nonreflecting boundary condition for the continuous equations. If for instance $A > 0$, then at the right boundary ($x = L$), all modes are outgoing, so no boundary condition is specified, and at the left boundary all solutions are incoming, so the nonreflecting boundary condition is merely $u(0, y, t) = 0$. When the equations are discretized, however, the problem is not trivial.

The analysis of the previous two sections shows that when the equations are discretized, spurious modes will be introduced which will travel in the opposite direction as the physical modes. Thus, n physical modes will still travel to the right, but now n spurious modes will travel to the left, and so it is important to use discrete nonreflecting boundary conditions at both boundaries to avoid numerical reflections.

Taking a Fourier–Laplace transform of (3.28), with (ik, s) the dual variables of (y, t), and defining $z = ik/s$ as before, we have

$$\hat{u}_x = -sM(z)\hat{u}, \tag{3.29}$$

where $M(z) = A^{-1}(I + zB)$. Now, we have an equation which resembles the one-dimensional system (3.4), except that now the matrix M is a function of z. This z-dependence carries through the analysis of Subsection 3.2 unaltered, so from Eqs. (3.20) and (3.22) we may immediately write down nonreflecting boundary closures for the discretized equations as

$$-sM(z)u_0 = \mathrm{d}_0^i u_0 \tag{3.30}$$

$$-sM(z)u_N = \mathrm{d}_N^o u_N, \tag{3.31}$$

where the operators d_0^i and d_N^o are defined by (3.23) and (3.21). Taking the inverse Fourier–Laplace transforms, we are left with

$$\frac{\partial u_0}{\partial t} + A\mathrm{d}_0^i u_0 + B\frac{\partial u_0}{\partial y} = 0 \tag{3.32}$$

$$\frac{\partial u_N}{\partial t} + A\mathrm{d}_N^o u_N + B\frac{\partial u_N}{\partial y} = 0 \tag{3.33}$$

which is exactly the form of the original Eq. (3.28) with the operators d_0^i and d_N^o taking the form of closures for the x-derivative. Typical boundary closures used for one-way equations (such as the Euler equations linearized about a supersonic flow) use $u_0 = 0$ in place of (3.32) and use a one-sided difference approximation to the x-derivative in place of d_N^o in (3.33). Such an ad hoc approach gives a greater reflection of physical waves into spurious waves at the downstream boundary, and *perfect reflection* of spurious waves into physical waves at the upstream boundary.

3.4. *Numerical Boundary Conditions for Two-Way Systems*

We now derive numerically nonreflecting boundary conditions for two-way systems, in which the continuous equations admit both rightgoing and leftgoing solutions. The idea is to use the boundary conditions for the continuous equations to decouple the two-way system into two one-way systems, and then to apply the discrete boundary conditions of the previous section to each one-way system.

Consider again the system (3.28), written in the transformed form

$$\hat{u}_x = -sM(z)\hat{u}$$

and assume for the moment that we have access to a pair of perfectly nonreflecting boundary conditions for the continuous equations, which we write (as in Section 2) as

$$\begin{aligned} E^{\mathrm{I}}\hat{u} &= 0, \qquad \text{at } x = 0 \\ E^{\mathrm{II}}\hat{u} &= 0, \qquad \text{at } x = L, \end{aligned} \tag{3.34}$$

where E^{I} and E^{II} may be functions of z. Now define the square matrix

$$E(z) = \begin{pmatrix} E^{\mathrm{I}} \\ E^{\mathrm{II}} \end{pmatrix}$$

and let $T(z)$ be the matrix of right eigenvectors of $M(z)$, arranged so that

$$T^{-1}MT = \Lambda = \begin{pmatrix} \Lambda^{\mathrm{I}} & 0 \\ 0 & \Lambda^{\mathrm{II}} \end{pmatrix}, \tag{3.35}$$

where Λ^{I} is positive-definite for $z = 0$ (rightgoing), and Λ^{II} is negative-definite for $z = 0$ (leftgoing). Since the boundary condition (3.34) is perfectly nonreflecting, it follows (see Subsection 2.1) that the matrix

$$C := ET = \begin{pmatrix} C^{\mathrm{I}} & 0 \\ 0 & C^{\mathrm{II}} \end{pmatrix} \tag{3.36}$$

is block diagonal. Furthermore, if both boundary conditions are well posed, it follows that C is invertible, and hence the square matrix E is invertible. We now use the matrix E to transform to a coordinate system where rightgoing and leftgoing modes are decoupled. Let $g = E\hat{u}$. Then

$$\frac{\mathrm{d}}{\mathrm{d}x} E\hat{u} = -s(EME^{-1})E\hat{u}, \qquad \text{i.e.,} \ \frac{\mathrm{d}}{\mathrm{d}x} g = -s\Phi g, \tag{3.37}$$

where

$$\begin{aligned} \Phi := EME^{-1} &= E(T\Lambda T^{-1})E^{-1} \\ &= C\Lambda C^{-1} \\ &= \begin{pmatrix} C^{\mathrm{I}} & 0 \\ 0 & C^{\mathrm{II}} \end{pmatrix} \begin{pmatrix} \Lambda^{\mathrm{I}} & 0 \\ 0 & \Lambda^{\mathrm{II}} \end{pmatrix} \begin{pmatrix} C^{\mathrm{I}^{-1}} & 0 \\ 0 & C^{\mathrm{II}^{-1}} \end{pmatrix} \\ &= \begin{pmatrix} \Phi^{\mathrm{I}} & 0 \\ 0 & \Phi^{\mathrm{II}} \end{pmatrix}. \end{aligned}$$

The eigenvalues of Φ^{I} and Φ^{II} are the same as the eigenvalues of Λ^{I} and Λ^{II}, respectively, so Eq. (3.37) is a system of two decoupled *one-way* equations

$$\begin{aligned} \frac{\mathrm{d}}{\mathrm{d}x} g^{\mathrm{I}} &= -s\Phi^{\mathrm{I}} g^{\mathrm{I}} \\ \frac{\mathrm{d}}{\mathrm{d}x} g^{\mathrm{II}} &= -s\Phi^{\mathrm{II}} g^{\mathrm{II}}, \end{aligned}$$

where the first equation has purely rightgoing solutions ($\Phi^{\mathrm{I}} > 0$ for $z = 0$), and the second equation has purely leftgoing solutions ($\Phi^{\mathrm{II}} < 0$ for $z = 0$). Since the rightgoing and leftgoing modes are now decoupled, we may apply the numerical boundary conditions from Section 3 to each equation. Introducing a regular grid in x with mesh spacing h and letting g_k denote $g(x = kh)$, at the left boundary $k = 0$ we may write the discrete (approximately) nonreflecting boundary condition

$$-s\Phi^{\mathrm{I}} g_0^{\mathrm{I}} = \mathrm{d}_0^i g_0^{\mathrm{I}} \tag{3.38}$$

$$-s\Phi^{\mathrm{II}} g_0^{\mathrm{II}} = \mathrm{d}_0^o g_0^{\mathrm{II}} \tag{3.39}$$

and at the right boundary $k = N$ we have the boundary condition

$$-s\Phi^{\mathrm{I}} g_N^{\mathrm{I}} = \mathrm{d}_N^o g_N^{\mathrm{I}} \tag{3.40}$$

$$-s\Phi^{\mathrm{II}} g_N^{\mathrm{II}} = \mathrm{d}_N^i g_N^{\mathrm{II}}. \tag{3.41}$$

As described in Subsection 3.2, these discrete boundary conditions are nonreflecting up to arbitrarily high-order accuracy as $h \to 0$, and note that this is the first approximation that has been made. Defining the matrix operators

$$\begin{aligned} D_L &= \begin{pmatrix} \mathrm{d}_0^i I & 0 \\ 0 & \mathrm{d}_0^o I \end{pmatrix} \\ D_R &= \begin{pmatrix} \mathrm{d}_N^o I & 0 \\ 0 & \mathrm{d}_N^i I \end{pmatrix}, \end{aligned} \tag{3.42}$$

where I denotes the identity matrix of appropriate dimension, and recalling that $g = E\hat{u}$ and $\Phi E = EM$, the boundary conditions become

$$\begin{aligned} -sE(z)M(z)\hat{u}_0 &= D_L E(z)\hat{u}_0 \\ -sE(z)M(z)\hat{u}_N &= D_R E(z)\hat{u}_N. \end{aligned} \tag{3.43}$$

So far, we have assumed that the boundary conditions (3.34) for the continuous equations were perfectly nonreflecting. For many examples, including the linearized Euler equations, the exact boundary conditions are nonlocal in space and time (i.e., the matrix $E(z)$ contains non-rational functions of z), so it may be desirable to replace $E(z)$ with an approximation $E'(z)$ that is rational. For the linearized Euler equations (cf. Subsection 2.2), this approximation corresponds to replacing $\gamma(z)$ with an approximation $r(z)$. When this approximation is introduced, the matrix C in (3.36) will not be exactly block diagonal, but will have small off-diagonal terms, and so the subsequent equations will not be perfectly decoupled, and errors will be introduced. The errors for such local, approximately nonreflecting boundary conditions can be analyzed, as follows, by considering the reflection coefficients.

3.4.1. Discrete reflection coefficients. Take the left boundary first and consider the approximately nonreflecting boundary condition

$$-sE'M\hat{u}_0 = D_L E'\hat{u}_0 \tag{3.44}$$

and transform to characteristic variables $f = T^{-1}\hat{u}$ to obtain

$$-sC\Lambda f_0 = D_L C f_0, \tag{3.45}$$

where now the matrix

$$C := E'T = \begin{pmatrix} C^{\mathrm{I}} & D^{\mathrm{I}} \\ D^{\mathrm{II}} & C^{\mathrm{II}} \end{pmatrix} \tag{3.46}$$

is not perfectly block diagonal. Writing (3.45) as

$$\begin{pmatrix} \mathrm{d}_0^i I & 0 \\ 0 & \mathrm{d}_0^o I \end{pmatrix} \begin{pmatrix} C^{\mathrm{I}} & D^{\mathrm{I}} \\ D^{\mathrm{II}} & C^{\mathrm{II}} \end{pmatrix} \begin{pmatrix} f_0^{\mathrm{I}} \\ f_0^{\mathrm{II}} \end{pmatrix} + s \begin{pmatrix} C^{\mathrm{I}} & D^{\mathrm{I}} \\ D^{\mathrm{II}} & C^{\mathrm{II}} \end{pmatrix} \begin{pmatrix} \Lambda^{\mathrm{I}} & 0 \\ 0 & \Lambda^{\mathrm{II}} \end{pmatrix} \begin{pmatrix} f_0^{\mathrm{I}} \\ f_0^{\mathrm{II}} \end{pmatrix} = 0 \tag{3.47}$$

and recalling from Subsection 2.1 the continuous reflection coefficient matrices $R^{\mathrm{I}} = -(C^{\mathrm{I}})^{-1}D^{\mathrm{I}}$ and $R^{\mathrm{II}} = -(C^{\mathrm{II}})^{-1}D^{\mathrm{II}}$, the boundary condition becomes

$$\left(\mathrm{d}_0^i + s\Lambda^{\mathrm{I}}\right) f_0^{\mathrm{I}} - R^{\mathrm{I}}\left(\mathrm{d}_0^i + s\Lambda^{\mathrm{II}}\right) f_0^{\mathrm{II}} = 0 \tag{3.48}$$

$$\left(\mathrm{d}_0^o + s\Lambda^{\mathrm{II}}\right) f_0^{\mathrm{II}} - R^{\mathrm{II}}\left(\mathrm{d}_0^o + s\Lambda^{\mathrm{I}}\right) f_0^{\mathrm{I}} = 0. \tag{3.49}$$

Since f^{I} are purely rightgoing modes and f^{II} are purely leftgoing modes, it is clear from these equations that when the reflection coefficient matrices are not identically zero, we are

applying the wrong numerical boundary condition to some of the waves at the boundary. For instance, in the second term of (3.48), we are incorrectly applying the d^i operator to an outgoing wave f^{II}, and in the second term of (3.49) we are applying the d^o operator to an incoming wave f^{I}. These are the terms that arise from imperfect decoupling and will cause reflections.

To proceed, we split the solution f into physical and spurious parts f^+ and f^-, as in Subsection 3.2. Since Λ is diagonal (with diagonal elements λ_j), we may easily write $(\mathrm{d}^i{}_0 + s\Lambda) f_0$ in terms of components

$$\begin{aligned}
\left(\mathrm{d}^i_0 + s\lambda_j\right)\left(f_0^{+j} + f_0^{-j}\right) &= -\frac{1}{c_1 h}\sum_{k=0}^{N_d} d_k\left(f_k^{+j} + f_k^{-j}\right) + s\lambda_j\left(f_0^{+j} + f_0^{-j}\right) \\
&= \frac{1}{c_1 h}\left(c_1 sh\lambda_j - \sum_{k=0}^{N_d} d_k(\kappa^{+j})^k\right) f_0^{+j} \\
&\quad - \frac{1}{c_1 h}\left(-c_1 sh\lambda_j + \sum_{k=0}^{N_d} d_k(\kappa^{-j})^k\right) f_0^{-j} \\
&= \frac{1}{c_1 h}\left(c(\phi_j)\, f_0^{+j} - d(\phi_j)\, f_0^{-j}\right),
\end{aligned} \tag{3.50}$$

where $\kappa^{\pm j}$ are the shift operators from Subsection 3.2, $c(\phi)$ and $d(\phi)$ are defined by (3.17), and $i\phi_j = sh\lambda_j$. Similarly, we have

$$\begin{aligned}
\left(\mathrm{d}^o_0 + s\lambda_j\right)\left(f_0^{+j} + f_0^{-j}\right) &= -\frac{1}{a_1 h}\left(\bar{a}(\phi_j)\, f_0^{+j} - \bar{b}(\phi_j)\, f_0^{-j}\right) \\
\left(\mathrm{d}^o_N + s\lambda_j\right)\left(f_N^{+j} + f_N^{-j}\right) &= -\frac{1}{c_1 h}\left(\bar{c}(\phi_j)\, f_N^{+j} - \bar{d}(\phi_j)\, f_N^{-j}\right) \\
\left(\mathrm{d}^i_N + s\lambda_j\right)\left(f_N^{+j} + f_N^{-j}\right) &= \frac{1}{a_1 h}\left(a(\phi_j)\, f_N^{+j} - b(\phi_j)\, f_N^{-j}\right),
\end{aligned} \tag{3.51}$$

where $a(\phi)$ and $b(\phi)$ are given by (3.19) and $\bar{a}$ denotes the complex conjugate of a. (Note that $\bar{\kappa}^{\pm j} = 1/\kappa^{\pm j}$ as long as $|\phi_j| \le \phi_c$.) Then (3.48) and (3.49) become

$$\begin{aligned}
C_1 f_0^{\mathrm{I}+} - D_1 f_0^{\mathrm{I}-} - R^{\mathrm{I}}\left(C_2 f_0^{\mathrm{II}+} - D_2 f_0^{\mathrm{II}-}\right) &= 0 \\
\bar{A}_2 f_0^{\mathrm{I}+} - \bar{B}_2 f_0^{\mathrm{I}-} - R^{\mathrm{I}}\left(\bar{A}_1 f_0^{\mathrm{II}+} - \bar{B}_2 f_0^{\mathrm{II}-}\right) &= 0,
\end{aligned} \tag{3.52}$$

where $\bar{A}_{1,2}$, $\bar{B}_{1,2}$, $C_{1,2}$, and $D_{1,2}$ are diagonal matrices of the form

$$\begin{aligned}
\bar{A}_1 &= \begin{pmatrix} \bar{a}(\phi_1) & & \\ & \ddots & \\ & & \bar{a}(\phi_l) \end{pmatrix}, \qquad \bar{A}_2 = \begin{pmatrix} \bar{a}(\phi_{l+1}) & & \\ & \ddots & \\ & & \bar{a}(\phi_n) \end{pmatrix} \\
C_1 &= \begin{pmatrix} c(\phi_1) & & \\ & \ddots & \\ & & c(\phi_l) \end{pmatrix}, \qquad C_2 = \begin{pmatrix} c(\phi_{l+1}) & & \\ & \ddots & \\ & & c(\phi_n) \end{pmatrix}, \text{ etc.}
\end{aligned} \tag{3.53}$$

Solving for the incoming modes in terms of the outgoing modes, we have

$$\begin{pmatrix} f_0^{\mathrm{I}+} \\ f_0^{\mathrm{II}-} \end{pmatrix} = \begin{pmatrix} I & C_1^{-1}R^{\mathrm{I}}D_2 \\ \bar{B}_2^{-1}R^{\mathrm{II}}\bar{A}_1 & I \end{pmatrix}^{-1} \begin{pmatrix} C_1^{-1}D_1 & C_1^{-1}R^{\mathrm{I}}C_2 \\ \bar{B}_2^{-1}R^{\mathrm{II}}\bar{B}_1 & \bar{B}_2^{-1}\bar{A}_2 \end{pmatrix} \begin{pmatrix} f_0^{\mathrm{I}-} \\ f_0^{\mathrm{II}+} \end{pmatrix}, \quad (3.54)$$

where the matrix on the right hand side is the matrix of reflection coefficients. An identical analysis for the right boundary condition

$$-sE'M\hat{u}_N = D_R E'\hat{u}_N \quad (3.55)$$

gives the reflection coefficients

$$\begin{pmatrix} f_N^{\mathrm{I}-} \\ f_N^{\mathrm{II}+} \end{pmatrix} = \begin{pmatrix} I & B_1^{-1}R^{\mathrm{I}}A_2 \\ \bar{C}_2^{-1}R^{\mathrm{II}}\bar{D}_1 & I \end{pmatrix}^{-1} \begin{pmatrix} B_1^{-1}A_1 & B_1^{-1}R^{\mathrm{I}}B_2 \\ \bar{C}_2^{-1}R^{\mathrm{II}}\bar{C}_1 & \bar{C}_2^{-1}\bar{D}_2 \end{pmatrix} \begin{pmatrix} f_0^{\mathrm{I}+} \\ f_0^{\mathrm{II}-} \end{pmatrix}. \quad (3.56)$$

Recall from Subsection 3.2.1. that the matrices $B^{-1}A$ and $C^{-1}D$ represent the *discrete* reflection coefficients for the given numerical boundary condition. As the *continuous* reflection coefficient matrices R^{I} and R^{II} go to zero, then, we retrieve the one-dimensional numerical reflection coefficients. If R^{I} and R^{II} are not zero, we may compute the necessary inverses using the general formula

$$\begin{pmatrix} I & X \\ Y & I \end{pmatrix}^{-1} = \begin{pmatrix} I + X\Delta^{-1}Y & -X\Delta^{-1} \\ -\Delta^{-1}Y & \Delta^{-1} \end{pmatrix} \quad (3.57)$$

as long as $\Delta = I - YX$ is invertible. For the local boundary conditions presented in Subsection 2.2 for the subsonic linearized Euler equations, the reflection coefficients at the left boundary are

$$\begin{pmatrix} f^{+1} \\ f^{+2} \\ f^{-3} \end{pmatrix} = \begin{pmatrix} \rho^i(\phi_1) & 0 & 0 \\ 0 & \rho^i(\phi_2)\frac{1}{\Delta_L}\left(1 - R_1R_2\frac{\bar{b}(\phi_2)d(\phi_3)}{b(\phi_3)\bar{d}(\phi_2)}\right) & R_1\frac{1}{\Delta_L}\left(\frac{c(\phi_3)}{c(\phi_2)} - \frac{\bar{a}(\phi_3)d(\phi_3)}{b(\phi_3)c(\phi_2)}\right) \\ 0 & R_2\frac{1}{\Delta_L}\left(\frac{\bar{b}(\phi_2)}{b(\phi_3)} - \frac{\bar{a}(\phi_2)d(\phi_2)}{b(\phi_3)c(\phi_2)}\right) & \bar{\rho}^o(\phi_3)\frac{1}{\Delta_L}\left(1 - R_1R_2\frac{\bar{a}(\phi_2)c(\phi_3)}{\bar{a}(\phi_3)c(\phi_2)}\right) \end{pmatrix} \begin{pmatrix} f^{-1} \\ f^{-2} \\ f^{+3} \end{pmatrix}, \quad (3.58)$$

where $\Delta_L = 1 - R_1R_2(\bar{a}(\phi_2)\,d(\phi_3))/(\bar{b}(\phi_3)c(\phi_2))$, and at the right boundary are

$$\begin{pmatrix} f^{-1} \\ f^{-2} \\ f^{+3} \end{pmatrix} = \begin{pmatrix} \rho^o(\phi_1) & 0 & 0 \\ 0 & \rho^o(\phi_2)\frac{1}{\Delta_R}\left(1 - R_1R_2\frac{a(\phi_3)\bar{c}(\phi_2)}{a(\phi_2)\bar{c}(\phi_3)}\right) & R_1\frac{1}{\Delta_R}\left(\frac{b(\phi_3)}{b(\phi_2)} - \frac{a(\phi_3)\bar{d}(\phi_3)}{b(\phi_2)\bar{c}(\phi_3)}\right) \\ 0 & R_2\frac{1}{\Delta_R}\left(\frac{\bar{c}(\phi_2)}{\bar{c}(\phi_3)} - \frac{a(\phi_2)\bar{d}(\phi_2)}{b(\phi_2)\bar{c}(\phi_3)}\right) & \bar{\rho}^l(\phi_3)\frac{1}{\Delta_R}\left(1 - R_1R_2\frac{b(\phi_3)\bar{d}(\phi_2)}{b(\phi_2)\bar{d}(\phi_3)}\right) \end{pmatrix} \begin{pmatrix} f^{+1} \\ f^{+2} \\ f^{-3} \end{pmatrix}, \quad (3.59)$$

where $\Delta_R = 1 - R_1R_2(a(\phi_3)\,\bar{d}(\phi_2))/(b(\phi_2)\bar{c}(\phi_3))$.

It is worth mentioning several features of the reflection coefficients given above. Of course, for the discrete system there are nine reflection coefficients at each boundary, while for the continuous system there are only two at each boundary (cf. Subsection 2.2.3). Note that the vorticity wave f^1 is perfectly decoupled from the acoustic waves f^2 and f^3, even

when the boundary conditions are discretized. This result may seem obvious, but it is *not* the case for typical ad hoc closures.

Note, however, that the continuous reflection coefficients R_1 and R_2 are multiplied by coefficients that depend on the numerical boundary closure used. Most of these coefficients (e.g., ρ^o, ρ^i) become smaller as the order of the numerical boundary conditions given in Table I increases. However, some of them increase, so we must be careful when deciding which numerical boundary condition to use. This point will be discussed further when test cases are presented in Section 4.

3.5. *Implementation of High-Order Boundary Conditions*

Even though the boundary conditions given by (3.44) and (3.55) are local, they involve potentially high-order derivatives in time and space. In order to implement them efficiently, it is desirable to write the high-order equations instead as systems of first-order equations. Goodrich and Hagstrom [8, 12] accomplish this by expanding rational functions in partial fractions and introducing state variables (auxiliary variables). We present an alternative approach, analagous to the standard method by which high-order ordinary differential equations are reduced to systems of first-order equations.

First, it is useful to rewrite the boundary conditions as closures for the x-derivative. A closure is necessary whenever an implicit finite-difference scheme is used, and formulating the boundary condition in this way is useful also for explicit schemes, as the boundary points are solved using the same equations as the interior points. Thus we use the interior equations

$$\hat{u}_x = -sM(z)\hat{u} = -sA^{-1}(I + zB)\hat{u} \tag{3.60}$$

to rewrite the boundary conditions (3.44) and (3.55) as the boundary closures

$$\begin{aligned} E'(z)\frac{\partial \hat{u}_0}{\partial x} &= D_L E'(z)\hat{u}_0 \\ E'(z)\frac{\partial \hat{u}_N}{\partial x} &= D_R E'(z)\hat{u}_N, \end{aligned} \tag{3.61}$$

where $\partial\hat{u}_0/\partial x$ and $\partial\hat{u}_N/\partial x$ denote the closures for the derivatives at the boundaries. Now, the matrix E' is a rational function of z, but by multiplying each row of this equation by its least common denominator we may obtain a new system that is polynomial in z,

$$\begin{aligned} E''(z)\frac{\partial \hat{u}_0}{\partial x} &= D_L E''(z)\hat{u}_0 \\ E''(z)\frac{\partial \hat{u}_N}{\partial x} &= D_R E''(z)\hat{u}_N, \end{aligned} \tag{3.62}$$

where now the matrix

$$E''(z) = E_0 + zE_1 + \cdots + z^p E_p \tag{3.63}$$

is a polynomial in z. If we were to multiply through by s^p and take the inverse Fourier and Laplace transforms, we would obtain partial differential equations for the closures $\partial\hat{u}_0/\partial x$ and $\partial\hat{u}_N/\partial x$ that involve high-order mixed partial derivatives. Instead, we may

write expressions for the closures that do not involve high-order derivatives in time and space by introducing auxiliary variables. At the left boundary, the closure (3.62) may be written

$$\begin{aligned} E_0\frac{\partial u_0}{\partial x} &= D_L E_0 u_0 + \frac{\partial}{\partial y}(F_0 u_0 + h_1) \\ \frac{\partial h_j}{\partial t} &= D_L E_j u_0 + \frac{\partial}{\partial y}(F_j u_0 + h_{j+1}), \qquad j = 1, \ldots, p-1 \\ \frac{\partial h_p}{\partial t} &= D_L E_p u_0 + \frac{\partial}{\partial y} F_p u_0, \end{aligned} \tag{3.64}$$

where $h_1, \ldots, h_p$ are state variables, and the matrices $F_0, \ldots, F_p$ are defined by

$$\begin{aligned} F_0 &= E_1 A^{-1} \\ F_j &= E_j A^{-1} B + E_{j+1} A^{-1}, \qquad j = 1, \ldots, p-1 \\ F_p &= E_p A^{-1} B. \end{aligned} \tag{3.65}$$

The right boundary closure for the point u_N may be treated similarly, with D_L replaced by D_R.

If $E'(z)$ is a rational function of degree (m, n), then the number of auxiliary variables required is $p = \max\{m, n+1\}$. If $m = n$ or $m = n+2$ (required for well-posedness), then the continuous reflection coefficients for the linearized Euler equations are $O(z^{2p})$ at the left boundary and $O(z^{2p+2})$ at the right boundary (cf. Subsection 2.2.4). For instance, if a (4,4) Padé approximation to $\gamma(z)$ is used, five state variables are needed at each boundary. Since the number of points N in a computation is typically one or two orders of magnitude greater than this, the additional computational cost for highly accurate boundary conditions is often negligible.

Additional details concerning implementation for the linearized Euler equations are available on our website, at `http://poisson.caltech.edu/cfda`.

4. TEST CASES

In this section we give the results of test problems that we have constructed to validate the numerically nonreflecting boundary conditions presented in the previous section and to illustrate some subtleties. Specifically, we have tested the discrete boundary conditions of Subsection 3.4 on the linearized Euler equations, using the continuous boundary conditions from Subsection 2.2, with several different rational function approximations for $\gamma(z)$ and several of the different schemes for boundary closures reported in Table I. In particular, we have considered the (0,0), (2,0), (2,2), (4,4), and (8,8) Padé approximations to γ. As mentioned in Subsection 2.2.4, the (0,0) approximation ($\gamma \approx 1$) is the one used by Giles in [7], and the (4,4) approximation is equivalent to the approximation used by Goodrich and Hagstrom in [9]. Finally, we have implemented a (4,4) rational function approximation that is chosen to interpolate the function $\gamma(z)$ at specific points, so that the resulting boundary condition is perfectly nonreflecting for waves at certain angles to the boundary. This approximation will be referred to as "(4,4) Interp" in the discussions below. The specific interpolation points are $z = 0,\ \pm 1/4,\ \pm 1/2,\ \pm 3/4,$ and ± 1, and were chosen to improve performance for nearly tangential waves.

In assessing the effects of the numerical nonreflecting boundary closures, it is useful to compare our schemes with a typical "ad hoc" boundary closure. In this closure, we attempt to reproduce what we believe is the standard way of implementing nonreflecting boundary conditions. That is, we implement (2.17) directly and use a 4th-order explicit closure for the finite difference in the x-direction whenever necessary.

In all tests, we compute the solution on a two-dimensional domain that is periodic in the y-direction. The fourth-order Padé scheme ($a = 3/4, \alpha = 1/4$) is used for the spatial derivatives, and 4th-order Runge–Kutta time advancement is used to advance all equations, boundary conditions, and state variables. We have observed that the CFL constraint of the scheme is unaffected by the boundary conditions or boundary closures, though we have no proof of this in the general case. The results given below all use a (maximum) CFL number of 1.

4.1. *Convection of a Vortex*

In the first test, we consider the propagation of a vortex in a uniform stream with $U = 1/2$. To avoid the slowly decaying tangential velocity associated with finite circulation in two dimensions, we chose an initial "sombrero" vorticity distribution that has zero total circulation,

$$\omega_z = \frac{1}{r}\frac{\partial}{\partial r}\left(r^2 e^{-(r/\alpha)^2}\right),$$

where $r = \sqrt{x^2 + y^2}$, in the computational domain $-10\alpha \le x, y \le 10\alpha$, with 101 grid points in each direction. In the plots, lengths are given with respect to α, and time is normalized by α and the sound speed of the base flow.

The continuous boundary conditions are exactly nonreflecting for the vorticity wave, independent of the choice of rational function approximation. Thus, all reflections will be spurious numerical waves, so this test is useful in assessing the effectiveness of the boundary closures from Table I, as compared with the ad hoc 4th-order closure.

Figure 3 shows the RMS value of the vorticity (over x and y) as a function of time. Near $t = 20$, the vortex is passing through the right boundary. If there were no spurious

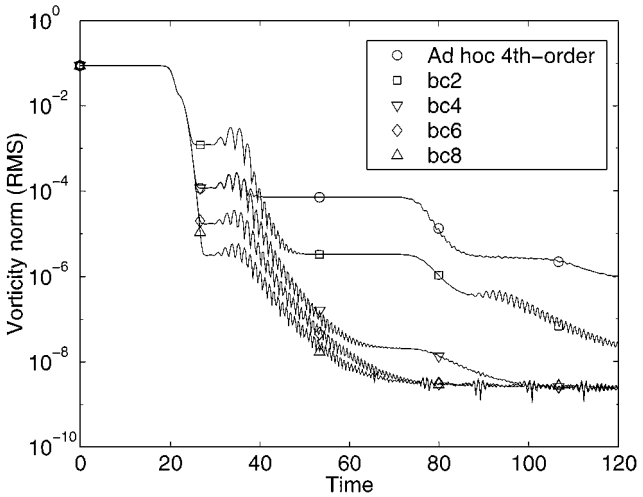

FIG. 3. Initial vortex. The RMS vorticity in the computational domain as a function of time for several different nonreflecting boundary closures (see Table I).

reflections, then the energy within the domain would decrease to zero. However, the exiting vorticity produces a spurious vorticity wave, which propagates upstream. The strength of this wave is evident between times 25 and 40 and is drastically reduced as the order of the boundary closure for the outgoing (smooth) waves (at $x = L$) is increased. The ad hoc boundary closure (which uses a fourth-order one-sided difference scheme for closure), produces the same results as boundary condition bc4 in this regime. However, the spurious wave eventually reflects at the upstream boundary, and the reflected energy is again greatly reduced by using the high order nonreflecting boundary closures. The ad hoc boundary closure shows perfect reflection of this spurious wave at the inflow boundary. Eventually, the energy stops decreasing for the high order closures, once most of the low-frequency waves (both physical and spurious) have left the domain and the error is dominated by waves near the critical frequency (recall from Subsection 3.2.1 that waves at the critical frequency always suffer pure reflection).

4.2. *Propagation of a Pressure Pulse*

In the next test, an initially Gaussian distribution of pressure spreads out as a cylindrical acoustic wave in the domain with a uniform velocity $U = 1/2$. This problem (on both periodic [9] and nonperiodic domains [23]) has been suggested several times as a test of the efficacy of boundary conditions, since the numerical solution may be compared to the exact solution, which may be solved by quadrature. In the present case, we compare with a reference solution we obtain by performing the computation on a much larger domain, until that time when it first becomes contaminated by reflections (physical or spurious) from the boundaries. This procedure is useful for isolating errors associated with the boundary conditions alone, since in the present case these can, for the most accurate boundary conditions, be smaller than other truncation errors.

The Gaussian pulse is initially given by $p = \exp -(r/\alpha)^2$, where α is the initial width of the pulse. Again the amplitude is unity, and α is used for the length scale in the nondimensionalization. The grid is identical to the one for the vortex test discussed above. In Fig. 4, pressure contours of the solution are plotted (top row) at several different times, and show the propagation of the wave. Since the domain is periodic, waves from images of the initial condition are evident beginning at time $t = 12$. By time $t = 20$, we see that a significant component of the wave motion corresponds to nearly glancing waves. (Note that for $U = 1/2$, waves whose group velocity is tangent to the boundary have wavefronts at an angle $\sin^{-1} U = 30^\circ$ to the horizontal.) As discussed at the end of Section 2, all of the rational function approximations in the continuous boundary conditions give pure reflection for waves that are tangent to the boundary.

Figure 4 also shows the error (difference between the computed solution and the reference solution) for several different boundary closures: the ad hoc boundary closure, and three nonreflecting closures, bc4.0, bc8, and bc8.0. The closure bc8 uses all coefficients from scheme bc8 in Table I, and the closures bc4.0 and bc8.0 use coefficients from schemes bc4 and bc8, respectively, everywhere except at the right boundary, where the incoming closure uses bc0. These closures are discussed in more detail below. All results in Fig. 4 are for a (4,4) Padé approximation for $\gamma(z)$.

In Fig. 4, at $t = 8$, the ad hoc closure shows a leftgoing spurious wave emanating from the right boundary as the physical pressure wave leaves the domain. The closure bc4.0 shows the same reflection, but for the higher order closures bc8 and bc8.0 this reflection is about two orders of magnitude smaller, too small to show up on the same contour levels. At time

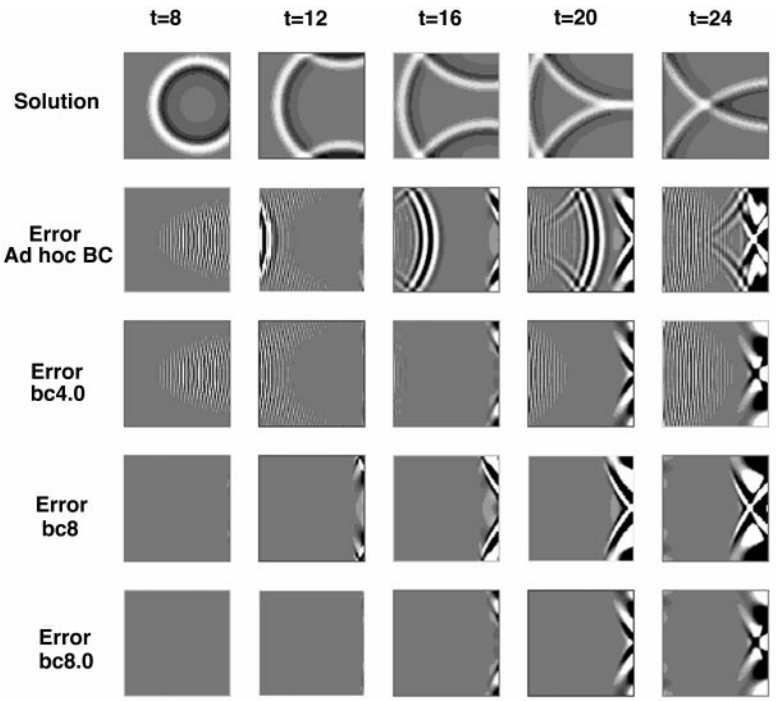

FIG. 4. Initial pressure pulse. Contours of the pressure (min -0.1, max 0.1) at several instants in time for the reference solution; contours of the error in the pressure (min -10^{-5}, max 10^{-5}) using a (4,4) Padé approximation for $\gamma(z)$, with the 4th-order ad hoc closure, and with discretely nonreflecting closures bc4.0, bc8, and bc8.0.

$t = 12$, the ad hoc closure shows the sawtooth spurious wave reflecting off the left boundary as a smooth, rightgoing physical wave. The initial pressure pulse still has not reached the left boundary. For bc4.0, even though the spurious wave leaving the left boundary has the same magnitude as it did for the ad hoc closure, the reflection into a physical wave is drastically reduced, so that by time $t = 16$ the closure bc4.0 shows no trace of the spurious wave, while the ad hoc closure has produced a conspicuous reflection, traveling to the right.

Also by this time, $t = 16$, a different sort of error is beginning to appear at the right boundary. This is the error from the continuous boundary condition, the error in the (4,4) Padé approximation for $\gamma(z)$. It propagates into the domain very slowly, as the only significant reflections are for waves whose group velocity is very small. Compared to the ad hoc closure, this error for closures bc4.0 and bc8.0 is slightly smaller, but for bc8 this error is noticeably larger. This effect is explained by the discrete reflection coefficients of Subsection 3.4.1 and is the motivation for the closures bc4.0 and bc8.0, discussed in more detail below.

By time $t = 20$, the initial pressure pulse reaches the left boundary and produces another spurious reflection, apparent in the ad hoc closure and in the closure bc4.0. Again, this reflection is much smaller for the closures bc8 and bc8.0, but the error at the right boundary (from the Padé approximation) is still larger for bc8. By time $t = 24$, this error overwhelms the error from spurious reflections, as the waves from the initial pressure pulse approach tangential incidence.

Performance of the ad hoc closure. Figure 5 shows the error from the 4th-order ad hoc closure, the standard way of discretizing nonreflecting boundary conditions, for various

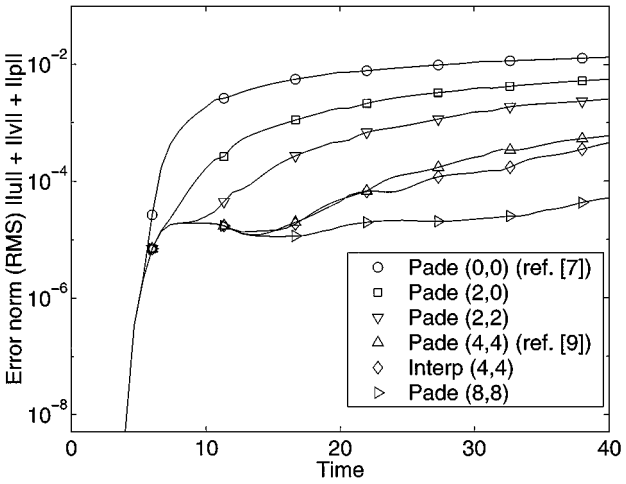

FIG. 5. Initial pressure pulse. The RMS error as a function of time for several different rational function approximations for $\gamma(z)$, all with a 4th-order ad hoc boundary closure.

rational function approximations for $\gamma(z)$. We plot the RMS value (over the computational domain) of the error between the numerical solution and the reference solution as a function of time.

At early times $t < 6$ when the acoustic wave is leaving the right boundary at nearly normal incidence, the error in all the boundary conditions is very small, but the error increases as the wave near the right boundary rotates away from normal incidence. Note that for $t < 15$, increasing the accuracy of the rational function approximation beyond a certain point does not further decrease the error. This error, starting at about $t = 8$, is the spurious wave reflected off the right boundary (clearly shown in Fig. 4), and the ad hoc closure is helpless to decrease this reflection, no matter how accurate the rational function approximation. For later times, of course, the more accurate boundary conditions perform better, as subsequent physical reflections are smaller, but the adverse effects of the spurious waves remain. If all four boundaries were nonreflecting, note that the wave would have left the right boundary by time $t = 12$ (cf. Fig. 4) so the error would be dominated by the spurious reflections. Thus, when an ad hoc closure is used, often there is little point in increasing the order of the rational function approximation beyond a certain point, as the error may be dominated by spurious reflections.

Performance of the discretely nonreflecting closures. In Fig. 6, we again plot the error between the numerical solution and the reference solution, but for several different numerical boundary closures from Table I, using both (0,0) and (4,4) Padé approximations for $\gamma(z)$. The closure bc8.0 is the same as shown in Fig. 4, described above.

Consider first the (4,4) Padé scheme (solid line), where the continuous reflection coefficients are small. At early times, the benefit of using the higher-order closures for the outgoing waves is evident. The initial "bump" in the curves centered around $t = 8$ is the spurious wave reflecting from the right boundary, as noted above. The amplitude of this error is decreased as the order of accuracy of the closure is increased. That is, schemes bc8 and bc8.0 give the best results, and using scheme bc2 gives the worst results, with the 4th-order ad hoc closure lying in between.

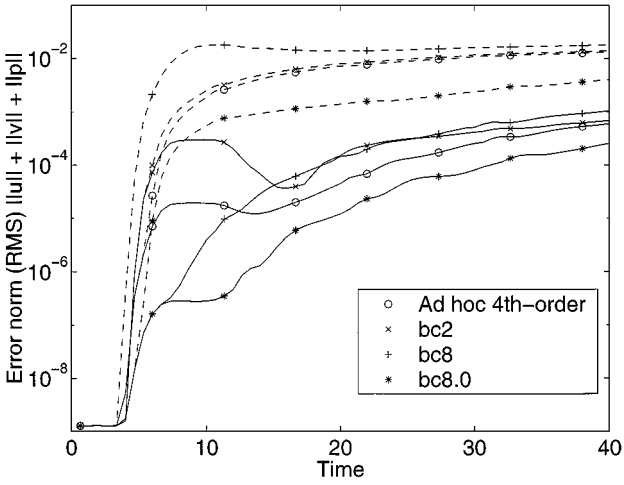

FIG. 6. Initial pressure pulse. The RMS error as a function of time for several boundary closures with a (0,0) Padé approximation for $\gamma(z)$, - - -; and a (4,4) Padé approximation, —.

For longer times, though, the difference between schemes bc8 and bc8.0 becomes apparent. The closure bc8.0 consistently performs best of all. For bc8, however, around time $t = 10$, the error starts to grow, soon exceeds the error from the ad hoc closure, and eventually performs worst of all!

This same effect is seen even more drastically when the (0,0) Padé scheme is used (dashed line). Here, at all times, scheme bc8.0 performs the best, but scheme bc8 performs worst of all.

A closer look at reflection coefficients. This surprising result is explained by the discrete reflection coefficients given by Eqs. (3.58) and (3.59). The numerically nonreflecting closures are designed to minimize the single-mode reflection coefficients ρ^o and ρ^i. More precisely, ρ^o decreases as the order of the d^o operator increases, and ρ^i decreases as the order of the d^i operator increases (see Fig. 2). These single-mode reflection coefficients are the dominant terms in the matrices of discrete reflection coefficients (3.58) and (3.59) as long as the *continuous* reflection coefficients R_1 and R_2 are small. However, if R_1 and R_2 are not small, the off-diagonal terms in these matrices become important.

For the closures given in Table I, some of these reflection coefficients *increase* as the order of the closures increases. In particular, the magnitude of $c(\phi_2)/c(\phi_3)$ increases as the order of the operator d^i increases, and the magnitude of $b(\phi_2)/b(\phi_3)$ increases as the order of the operator d^o increases. At the left boundary, the term $b(\phi_2)/b(\phi_3)$ multiplies the continuous reflection coefficient R_2 in the reflection coefficient from a leftgoing spurious acoustic wave to a rightgoing spurious acoustic wave, so increasing the order of the outgoing closure d^o will increase this reflection. At the right boundary, the term $c(\phi_2)/c(\phi_3)$ multiplies the continuous reflection coefficient R_2 in the reflection coefficient from a rightgoing acoustic wave to a leftgoing acoustic wave. Thus, increasing the order of the closures will increase these two reflections. This effect is evident whenever the rational function approximation breaks down and the continuous reflection coefficient R_2 is not small: in our case, this happens when a low-order approximation to $\gamma(z)$ is used, or for long times, when waves near the boundary are nearly tangent to the boundary.

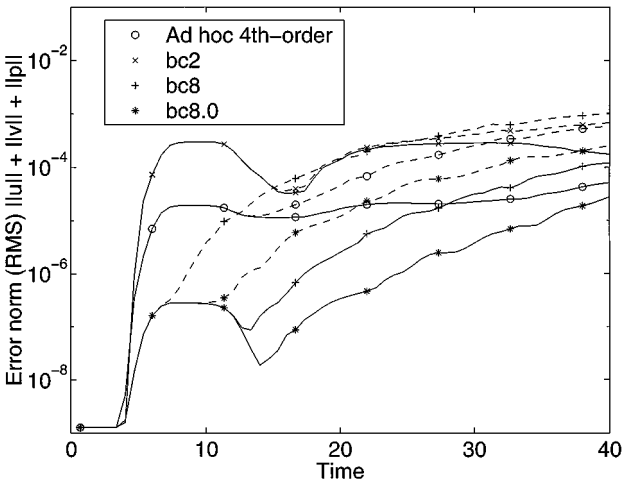

FIG. 7. Initial pressure pulse. The RMS error as a function of time for several boundary closures with a (4,4) Padé approximation for $\gamma(z)$, - - -; and an (8,8) Padé approximation, —.

Understanding these tradeoffs, we may carefully choose which closure to use at each boundary to produce the most accurate boundary condition for a specific problem. For the present test case, if initially no spurious waves are present (i.e., the initial condition is well resolved) then the *primary* reflections will be physical waves reflecting as spurious waves. At the right boundary, to make the primary reflection coefficients as small as possible, we should make ρ^o and $c(\phi_2)/c(\phi_3)$ as small as possible. To make ρ^o small, we use bc8 for the operator d^o, and to make $c(\phi_2)/c(\phi_3)$ small, we use bc0 for the operator d^i. We choose bc0 for the operator d^i at the expense of increasing reflections of spurious waves at the right boundary (increasing ρ^i), but these reflections are less important, as they will be *secondary* reflections.

At the left boundary, to make the primary reflection coefficients small we should make ρ^o as small as possible by using bc8 for d^o, and also $c(\phi_3)/c(\phi_2)$ small by using bc8 for d^i. The resulting boundary condition is labeled bc8.0 in the previous figures. As we expect, this carefully constructed boundary condition produces the smallest error.

High-order rational functions and high-order closures. Figure 7 shows the error for several closures, when a high order (8,8) Padé approximation is used (solid line), compared to a (4,4) Padé approximation (dashed line).

For early times ($t < 20$), before the waves are close to tangential incidence, increasing the rational function approximation improves the error little, if at all, for the lower order closures (the ad hoc closure and bc2) because the error is dominated by spurious waves. For the higher order closures bc8 and bc8.0, however, increasing the rational function approximation significantly improves the error, since here the spurious reflections are small and the continuous reflection coefficients are important.

Finally, we add that many physically realistic acoustic fields will not involve waves near glancing incidence, and in those cases uniformly more accurate results are obtained as the order of the nonreflecting boundary closure is increased.

Comparison with other truncation errors. We mentioned earlier that the boundary errors can be smaller than other truncation errors. This is especially true for the reflections of spurious waves, which are reduced as some power of h as $h \to 0$. For nearly tangential waves,

where the boundary error comes from a breakdown of the rational function approximation, the error is much larger than other truncation errors, and does not scale with h.

For the 4th-order ad hoc boundary condition, for early times ($t < 20$) the boundary errors shown in Fig. 4 are smaller than the other truncation errors (although of the same order). One might then question why we should be concerned with such small errors. Although the spurious reflections are smaller than the other truncation errors, they are much more insidious. The other truncation errors consist entirely of phase and amplitude error, and in a non-periodic problem, they will eventually leave the domain, while the boundary errors will reflect back and forth and persist indefinitely. Furthermore, in a sensitive computation such as an aeroacoustic computation of a flow with self-sustained oscillations, these reflections may be amplified and cause the flow to oscillate at non-physical frequencies, while amplitude and phase errors are more benign and do not cause such qualitatively different behavior.

5. CONCLUSIONS

We have developed a framework for constructing local, strongly well-posed boundary conditions for finite-difference solutions of linear hyperbolic systems. These boundary conditions take explicit account of the dispersive character of the finite-difference approximation and are designed to minimize the reflection of spurious waves at the boundaries. As such, they are dependent on the particular finite-difference scheme, and we have used a 3-point Padé centered-difference scheme to illustrate the analysis. The analysis leads to boundary closures to the finite-difference scheme, and different closures need to be applied to incoming and outgoing waves at each boundary.

When these discrete boundary conditions are applied to the Euler equations, linearized about a subsonic flow, the local boundary conditions rely on a rational function approximation to the function $\sqrt{1-z^2}$, which is obtained when waves are decomposed into rightgoing and leftgoing modes in Fourier space. As in previous boundary conditions [27] for the simple wave equation, we have shown that several classes of rational function approximations lead to stable, well-posed boundary conditions. The scheme can thus be extended to arbitrarily high order of accuracy.

Numerical experiments using these boundary conditions for the linearized Euler equations verify that usually, high-order numerical closures produce smaller reflections than low-order closures or ad hoc closures. For vorticity waves leaving the boundary, for instance, higher order closures always work better. However, there can exist situations where the higher-order boundary closures can amplify reflections due to approximations in the continuous boundary conditions. For the linearized Euler equations, for instance, using a high-order closure for the incoming operator d^i at the right boundary amplifies errors from the continuous boundary conditions. Thus for the linearized Euler equations, one should generally use the closure bc0 from Table I for the incoming operator at the right boundary, and high-order closures everywhere else.

To summarize the results of the numerical experiments, if a low-order numerical closure is used, increasing the order of the approximation to $\gamma(z)$ beyond a certain point does not improve results, because the error will be dominated by spurious waves. Conversely, if a low-order approximation for $\gamma(z)$ is used, then increasing the order of the discrete closure beyond a certain point does not improve results, because the error will be dominated by reflections of physical waves. High-order closures and high-order rational function approximations are used most effectively when used together.

We note that the spurious numerical reflections addressed by these boundary conditions may also be reduced by adding small amounts of artificial viscosity, or numerical smoothing, as one reviewer pointed out. However, artificial viscosity, when added in quantities sufficient to damp the spurious waves, will also have a significant effect on the smooth waves with relatively few (5–10) points per wavelength, and thereby degrade the accuracy of the high-order schemes. The boundary conditions presented in this paper effectively reduce the spurious waves without degrading the accuracy of the method.

Though we have assumed in the analysis that we are dealing with constant coefficient linear equations, this is a necessary restriction only in a local region near the computational boundary. Thus the present boundary conditions can be used in computations where the far-field is governed by the linearized Euler equations, but more complicated (nonlinear or non-constant coefficient) equations are needed for an interior region. Moreover, they can be used on non-uniform meshes, provided that the mesh becomes approximately uniform in the vicinity of the boundary.

In the future, we intend to apply these boundary conditions to more complicated problems. Generalizing these boundary conditions to a single boundary in three dimensions is straightforward and including systems with uniformly characteristic boundary, such as Maxwell's equations, will be addressed in a forthcoming paper. A more complicated issue is how to deal with corners in two dimensions, and corners and edges in three dimensions. In addition, there is an urgent need for accurate boundary conditions for nonlinear equations where the nonlinearities near the boundary cannot be ignored (as in a turbulent outflow). We hope that having provided a general framework, wherein *all the errors due to artificial boundary conditions* have been analyzed, will aid in the development of techniques for more complex situations.

APPENDIX

We claim that if a matrix $N(i\omega, \kappa)$ is defined by

$$N(i\omega, \kappa) = \kappa^2(aI + \alpha i\omega hA) + \kappa(i\omega hA) - (aI - \alpha i\omega hA)$$

and $\kappa^{\pm}$ satisfies

$$(\kappa^{\pm})^2(a + \alpha i\omega h\lambda) + \kappa^{\pm} i\omega h\lambda - (a - \alpha i\omega h\lambda) = 0$$

then

$$N(i\omega, \kappa^{\pm})u = 0 \Leftrightarrow Au = \lambda u.$$

Proof. ($\Leftarrow$) Assume $Au = \lambda u$. Then

$$\begin{aligned} N(i\omega, \kappa^{\pm})u &= [(\kappa^{\pm})^2(aI + \alpha i\omega hA) + \kappa^{\pm}(i\omega hA) - (aI - \alpha i\omega hA)]u \\ &= [(\kappa^{\pm})^2(a + \alpha i\omega h\lambda) + \kappa^{\pm}(i\omega h\lambda) - (a - \alpha i\omega h\lambda)]u \\ &= 0u \end{aligned}$$

by definition of $\kappa^{\pm}$.

($\Rightarrow$) If $N(i\omega, \kappa^{\pm})u = 0$, then

$$[(\kappa^{\pm})^2(aI + \alpha i\omega hA) + \kappa^{\pm}(i\omega hA) - (aI - \alpha i\omega hA)]u = 0. \tag{A.1}$$

By definition of $\kappa^{\pm}$, for any u we have

$$[(\kappa^{\pm})^2(a + \alpha i\omega h\lambda) + \kappa^{\pm}(i\omega h\lambda) - (a - \alpha i\omega h\lambda)]u = 0. \tag{A.2}$$

Subtracting (A.2) from (A.1) gives

$$[(\kappa^{\pm})^2\alpha i\omega h(A - \lambda I) + \kappa^{\pm} i\omega h(A - \lambda I) + \alpha i\omega h(A - \lambda I)]u = 0$$
$$\Leftrightarrow [(\kappa^{\pm})^2\alpha + \kappa^{\pm} + \alpha](A - \lambda I)u = 0.$$

The coefficient in brackets is never zero if the implicit finite-difference scheme is non-singular, so we have $Au = \lambda u$, which was to be shown. ■

REFERENCES

1. A. Bayliss and E. Turkel, Far field boundary conditions for compressible flows, *J. Comput. Phys.* **48**, 182 (1982).
2. M. H. Carpenter, D. Gottlieb, and S. Abarbanel, Time-stable boundary conditions for finite-difference schemes solving hyperbolic systems: Methodology and application to high-order compact schemes, *J. Comput. Phys.* **111**, 220 (1994).
3. T. Colonius, Numerically nonreflecting boundary and interface conditions for compressible flow and aeroacoustic computations, *AIAA J.* **35**(7), 1126 (1997).
4. T. Colonius, S. K. Lele, and P. Moin, Boundary conditions for direct computation of aerodynamic sound generation, *AIAA J.* **31**(9), 1574 (1993).
5. B. Engquist and A. Majda, Absorbing boundary conditions for the numerical simulation of waves. *Math. Comp.* **31**(139), 629 (1977).
6. B. Engquist and A. Majda, Radiation boundary conditions for acoustic and elastic wave calculations, *Comm. Pure Appl. Math.* **32**, 313 (1979).
7. M. B. Giles, Nonreflecting boundary-conditions for Euler equation calculations, *AIAA J.* **28**(12), 2050 (1990).
8. J. W. Goodrich and T. Hagstrom, *Accurate Algorithms and Radiation Boundary Conditions for Linearized Euler Equations*, AIAA Paper 96-1660, 1996.
9. J. W. Goodrich and T. Hagstrom, *A Comparison of Two Accurate Boundary Treatments for Computational Aeroacoustics*, AIAA Paper 97-1585, 1997.
10. M. J. Grote and J. B. Keller, Exact nonreflecting boundary conditions for the time dependent wave equation, *SIAM J. Appl. Math.* **55**(2), 207 (1995).
11. B. Gustafsson, H.-O. Kreiss, and J. Oliger, *Time Dependent Problems and Difference Methods*, Pure and Applied Mathematics (Wiley, New York, 1995).
12. T. Hagstrom, On high-order radiation boundary conditions, *in* IMA Volume on Computational Wave Propagation (Springer-Verlag, New York/Berlin, 1996), p. 1.
13. J. S. Hesthaven, On the analysis and construction of perfectly matched layers for the linearized Euler equations, *J. Comput. Phys.* **142**(1), 129 (1998).
14. R. L. Higdon, Initial-boundary value problems for linear hyperbolic systems, *SIAM Rev.* **28**(2), 177 (1986).
15. R. Hixon, S.-H. Shih, and R. R. Mankbadi, Evaluation of boundary conditions for computational aeroacoustics, *AIAA J.* **33**(11), 2006 (1995).
16. C.-M. Ho, Y. Zohar, J. K. Foss, and J. C. Buell, Phase decorrelation of coherent structures in a free shear layer, *J. Fluid Mech.* **220**, 319 (1991).

17. F. Q. Hu, Absorbing boundary conditions for linearized Euler equations by a perfectly matched layer, *J. Comput. Phys.* **129**, 201 (1996).
18. H.-O. Kreiss, Initial boundary value problems for hyperbolic systems, *Comm. Pure Appl. Math.* **23**, 277 (1970).
19. S. K. Lele, Compact finite difference schemes with spectral-like resolution, *J. Comput. Phys.* **103**(1), 16 (1992).
20. S. K. Lele, *Computational Aeroacoustics: A Review*, AIAA Paper 97-0018, 1997.
21. A. Majda and S. Osher, Initial-boundary value problems for hyperbolic equations with uniformly characteristic boundary, *Comm. Pure Appl. Math.* **28**, 607 (1975).
22. C. K. W. Tam, *Advances in Numerical Boundary Conditions for Computational Aeroacoustics*, AIAA Paper 97-1774, 1997.
23. C. K. W. Tam and J. C. Webb, Dispersion-relation-preserving finite difference schemes for computational acoustics, *J. Comput. Phys.* **107**, 262 (1993).
24. C. K. W. Tam and J. C. Webb, Radiation boundary condition and anisotropy correction for finite difference solutions of the Helmholtz equation, *J. Comput. Phys.* **113**(1), 122 (1994).
25. K. W. Thompson, Time dependent boundary conditions for hyperbolic systems, *J. Comput. Phys.* **68**(1), 1 (1987).
26. L. N. Trefethen, Group velocity in finite difference schemes, *SIAM Rev.* **24**(2), 113 (1982).
27. L. N. Trefethen and L. Halpern, Well-posedness of one-way wave equations and absorbing boundary conditions, *Math. Comp.* **47**(176), 421 (1986).
28. S. V. Tsynkov, Numerical solution of problems on unbounded domains. *Appl. Numer. Math.* **27**(4), 465 (1998).
29. R. Vichnevetsky, Wave propagation analysis of difference schemes for hyperbolic equations: A review, *Int. J. Numer. Methods Fluids* **7**, 409 (1987).